PERFORMANCE ENHANCEMENT AND EMISSIONS REDUCTION IN A DIESEL ENGINE USING OLEANDER AND CROTON BIODIESEL DOPED WITH GRAPHENE NANOPARTICLES

TREZA WAMBUI

MASTER OF SCIENCE

(Energy Technology)

JOMO KENYATTA UNIVERSITY

OF

AGRICULTURE AND TECHNOLOGY

2023

Performance Enhancement and Emissions Reduction in a Diesel Engine Using Oleander and Croton Biodiesel Doped With Graphene Nanoparticles

Treza Wambui

A Thesis Submitted in Partial Fulfilment of the Requirements for the Degree of Master of Science in Energy Technology of the Jomo Kenyatta University of Agriculture and Technology

2023

DECLARATION

This thesis is my original work and has not been submitted for a degree in any other University

Signature…….…..Date……

Treza Wambui

This thesis has been submitted for examination with our approval as the University supervisors

Signature …….….. Date……

Prof. Ngugi Kamau, PhD

JKUAT, Kenya

Signature…….…..Date……

Dr. Francis Njoka, PhD

KU, Kenya

Signature…….…..Date……

Dr. Meshack Hawi, PhD

JKUAT, Kenya

DEDICATION

This work is wholeheartedly dedicated to my loving Son, **Solomon Kuria** who has been my source of inspiration and strength. A special feeling of gratitude to my late Mom, **Jane Njeri** (may her soul rest in eternal peace) who gave the little she had to ensure I had an opportunity to education.

To God be the glory.

ACKNOWLEDGMENTS

I wish to thank the Almighty God for being my strength, and guide and for enabling me to complete this research work. I am deeply indebted to my Supervisors Prof. Joseph Kamau, Dr. Meshack Hawi and Dr. Francis Njoka for their continuous guidance, selfless dissemination of information, supervision, insightful comments and encouragement throughout the course of my study. I wish to express my sincere appreciation to Japan International Corporation Agency (JICA) through AFRICA-ai-JAPAN Project and the Pan African University Institute for Basic Sciences, Technology and Innovation (PAUSTI) for funding the project. My special thanks go to Mr. Joseph Muigai, Mr. Eric Waiyaki and Mr. Eric Muthiani for their assistance during the experimental phase. Last but not least, I wish to thank Jomo Kenyatta University of Agriculture and Technology (JKUAT) for the provision of laboratory facilities.

TABLE OF CONTENTS

LIST OF TABLES

LIST OF FIGURES

LIST OF APPENDICES

LIST OF ABBREVIATIONS

AFDC	Alternative fuels data centre
ASTM	American Society for Testing and Materials
BSFC	Brake Specific Fuel Consumption.
BTDC	Before top dead centre
BTE	Brake Thermal Efficiency
B30	30% Palm Oil Biodiesel and 70% Diesel
B30GNPDMC10	B30 + GNPs +10% Dimethyl Carbonate
B30GNP40DMC10	B30 + 40 ppm GNPs +10% Dimethyl Carbonate
B30GNP80DMC10	B30 + 80 ppm GNPs +10% Dimethyl Carbonate
B30GNP120DMC10	B30 + 120 ppm GNPs +10% Dimethyl Carbonate
CI	Compression Ignition
CME	Croton Oil Methylester
CMO	Croton Megalocarpus Oil
CNO	Croton Nut Oil
CNT	Carbon Nanotubes
CO	Carbon Monoxide
CO_2	Carbon Dioxide
COPD	Chronic obstructive pulmonary disease
CV	Calorific Value
CVD	Chemical vapor deposition
DAQ	Data Acquisition Card
DMC	Dimethyl Carbonate
DMC10	10% Dimethyl Carbonate
D100	100% Neat Diesel
ECU	Engine Control Unit
EGT	Exhaust Gas Temperature
EN	European standards
FFA	Free fatty acids

GNPs	Graphene Nanoparticles
GHG	Greenhouse gas
GNP50OCB20	50ppm Graphene Nanoparticles + OCB20
GNP75OCB20	75ppm Graphene Nanoparticles + OCB20
GNP100OCB20	100ppm Graphene Nanoparticles + OCB20
GONPs	Graphene Oxide Nanoplatelets
HC	Hydrocarbons
HOME	Honge Oil Methyl Ester
IEA	International Energy Agency
JME20	20% JME +80% Diesel
KOH	Potassium hydroxide
Mg/L	Milligrams per litre
MWCNT	Multiwall carbon nanotubes
NaOH	Sodium hydroxide
NOx	Oxides of Nitrogen
O_2	Oxygen
OCB	Oleander Croton Biodiesel
OCB20	20% Oleander and Croton Biodiesel + 80% Diesel
PAHs	Polycyclic Aromatic Hydrocarbons
PC	Personal computer
PPM	Parts per million
RPM	Revolutions per minute
SWCNT	Single wall carbon nanotubes
TDC	Top dead center
UHC	Unburned Hydrocarbon
UNFCCC	United Nations Convention for Climate Change
WCOME	Waste Cooking Oil Methyl Ester
WHO	World Health Organization
YOME	Yellow Oleander Methyl Ester

ABSTRACT

Biodiesel is considered a suitable substitute to petroleum diesel because it is renewable, environment-friendly, and has a low carbon footprint. However, operation of a diesel engine with biodiesel has a few shortcomings, which include, poor atomization, clogging of fuel lines, incomplete combustion, fuel gelling during cold weather, and carbon deposits in the engine, which prevents it from replacing petroleum diesel completely. This study investigates the performance and emission characteristics of a compression ignition engine operating on Oleander and Croton biodiesel doped with graphene nanoparticles. Five fuel samples were used, including diesel (D100), diesel - 80% blended with Oleander and Croton biodiesel - 20% (OCB20) and OCB20 dosed with Graphene nanoparticles at mass fractions of 50 ppm (mg/L), 75 ppm (mg/L) and 100 ppm (mg/L), respectively. The chemical composition of biodiesel and graphene nanoparticles was analyzed using Fourier Transform Infrared (FTIR) spectroscopy while the morphology of the nanoparticles was analyzed using Scanning Electron Microscope (SEM). Engine tests revealed a significant improvement in brake thermal efficiency, especially at 75 ppm concentration which was 2.76% and 18.93% higher than diesel and OCB20, respectively, and a reduction in brake specific fuel consumption by 2.44% and 16.67% compared to diesel and OCB20, respectively. Carbon monoxide (CO) and unburnt hydrocarbon emissions (UHC) decreases for the 50 ppm sample, recording 8.58% and 21.65% reduction in CO and 52.2% and 50% in UHC compared to the diesel and OCB20, respectively. However, Oxides of Nitrogen (NOx) emissions increased. The results indicate that graphene nanoparticle-enhanced biodiesel can adequately substitute petroleum diesel, albeit with NOx reduction techniques.

CHAPTER ONE

INTRODUCTION

1.1 Background of the Study

Decline in fuel reserves, global industrialization, increase in the number of vehicles on the road and the ever-growing world population have led to increased energy demand, especially for diesel engines, which are used widely in different sectors including power generation, automobile and industrial applications. Diesel engines are robust, more durable and have low fuel consumption compared to spark ignition engines, making them more attractive for most commercial applications. However, petroleum diesel is non-renewable and is associated with air pollution and global warming.

Due to the pressing energy concerns, health and environmental impacts, several researchers have investigated exhaust gas emission reduction techniques, including exhaust gas after-treatment, engine modification, combustion management and use of alternative fuels and fuel additives. Recent studies have shown that biodiesel fuel is a promising substitute for petroleum diesel since it is not only environment-friendly and renewable but also biodegradable (Yarkasuwa, Wilson, & Michael, 2013). Sulphur free, oxygenated (Pattanaik Jena, & Misra, 2017) and has a low carbon footprint (Hanaki & Portugal-Pereira, 2018). Additionally, biodiesel is a good lubricant, thus reducing the tear and wear of the engine parts (Fazal Haseeb & Masjuki, 2013). Besides, its application does not require any engine modification.

Biodiesel is derived from animal fats and edible and non-edible oil feedstock such as Croton, Sunflower, Oleander and Castor oils through transesterification process. Oils from non-edible and drought-resistant feedstock are recommended to guard against food insecurity and reduce land competition with edible oil plants (Bhattacharyya, 2022). However, the performance of diesel engines run on biodiesel is a little inferior relative to fossil diesel owing to its high viscosity, high density and low heating value, which, if applied directly in compression ignition (CI) engines or in high proportion in diesel-biodiesel blends may lead to clogging of fuel lines, poor atomization and incomplete combustion as well as carbon deposits in the engine (Agarwal, Gupta, &

Dhar, 2017). Recent studies have shown that certain fuel additives in the form of nanoparticles

(NPs) can enhance combustion while reducing emissions from diesel engines. Hence, many researchers have tested the application of different metal-based and non-metal NPs to enhance biodiesel combustion while reducing exhaust emissions (Devarajan *et al.,* 2018). High thermal conductivity coupled with exceptionally high surface area per unit volume possessed by NPs provides a wide dynamic surface for chemical reactions which improves combustion and reduces exhaust emissions (Mahdi & Nsofor, 2017). However, due to environmental and health concerns on the effect of metal-based NPs, non-metal NPs and specifically carbon-based NPs have gained prominence (Goswami, Kim, Deep, Das, Bhattacharya, Kumar, & Adelodun, 2017) since they are devoid of any metal components, with a host of desirable chemical, physical, mechanical, and electrical characteristics. These additives possess attractive attributes such as excellent thermal conductivity and high surface area which makes them preferred candidates for biodiesel nano additives (El-Seesy, Hassan, & Ookawara, 2018).

Carbon-based NPs participate in exothermic reactions thus increasing the total released heat that eventually increases the calorific value of the base fuel (SiSim, H. S., Yetter, R. A., Connell, T. L., Dabbs, D. M., & Aksay, 2020). Carbon-based nano-additives form a long-term stable dispersion in the base fuels with minimal particle agglomeration compared to metallic additives and thus do not necessarily require the use of a surfactant (Soudagar, Nik-Ghazali, Abul Kalam, Badruddin, Banapurmath, & Akram 2018). They are also combustible and therefore do not form any deposits in the CI engines hence reducing the chances of fuel system blockage, unlike metal-based NPs which may get deposited in engine components.

Graphene is one of the common organic additives considered by most researchers in recent decades owing to its remarkable properties which include high thermal conductivity of about 3000–5000 W/m/K (Sang, Shin, Kim, & Yu, 2019), high electron mobility, high electrical conductivity and lightweight (Tony Pallone, 2018). Graphene is an allotrope of carbon, one atom thick with a 2D structure consisting of sp^2 bond. It has a high theoretical surface area of 2629 m^2/g (Igor Ivanov, 2019) the highest of all

known materials which provides a wide dynamic surface for chemical reactions which improves combustion and reduces exhaust emissions (Mahdi & Nsofor, 2017). The small particle size coupled with the low density which is 2.0-2.25 g/cm^3 (Daud, Hamidi & Mamat 2022) makes it easily dissolvable in many hydrocarbon fuels without agglomerating, thereby forming stable colloids with the base fluid (Chehroudi, 2016).

Graphene is preferred over other carbon-based nano additives such as graphene oxide and multiwall carbon tubes (MWCT) because of its high calorific value (CV), superior engine performance and low emissions (EL-Seesy & Hassan, 2019). The doped GNPs are converted to CO_2 during combustion and taken up by plants during photosynthesis, unlike metal-based NPs which are emitted directly from the exhaust to the environment, causing environmental pollution. Because GNPs are fully oxidized in high-temperature combustion regions with nearly no additional residues other than the common combustion products, they can be regarded as fuel supplements that not only contribute towards energy density but also environment-friendly.

In this work, Oleander and Croton oils are considered suitable feedstock for the synthesis of biodiesel since they are non-edible oils and therefore pose no threat to food security. In addition, the crops are drought resistant and can be grown on marginal land. Yellow Oleander seeds have a high oil content of more than 60% and a biodiesel yield of more than 80% and therefore can be harvested for large-scale biodiesel production (Yarkasuwa *et al.,* 2013). However, Yellow Oleander Methyl Ester (YOME) is not preferred for application in cold regions owing to its high cloud and pour points which are 12 ℃ and 2 ℃ respectively (Oseni & Obetta, 2012) which are higher compared to those of conventional diesel of 4 ℃ and -2 ℃, respectively (Osawa, Onyari, Sahoo, & Mulaa, 2014). On the other hand, Croton megalocarpus oil (CMO) has remarkable cold flow properties of -1.5 ℃ - cloud point and -6.5 ℃- pour point, which has rendered it useful in cold regions (Osawa *et al.,* 2014). However, the low seed yield and low oil content render Croton feedstock unsustainable. From the foregoing, biodiesel from the two feedstocks complement each other.

The nanofuel produced can be run on other engine models, as was confirmed by Jeyaseelan & Chako, (2020) who investigated performance and emission

characteristics of a twin-cylinder, four-stroke turbocharged diesel engine operated on *karanja* and waste cooking biodiesel-diesel blend doped with graphene oxide (GO) and graphene nanoplatelets (GNP).

1.2 Statement of the Problem

Rapid growth in global industrialization, population and high living standards have led to enormous increase in the demand and cost of energy, especially for fossils diesel, which is commonly used in transport sector and prime movers, power generation, manufacturing plants and construction industries because it is more economical compared to petrol. Moreover, diesel engines are robust and more durable compared to gasoline engines. However, petroleum diesel is non-renewable, it is foreign and as such the importing countries incur huge losses in foreign exchange, its combustion releases GHGs that largely contribute to global warming and it is not environment-friendly because it leads to emission of significant quantities of UHC, CO, soot and NOx which are harmful to the environment.

Biodiesel has emerged as a suitable substitute to petroleum diesel because it is renewable, biodegradable, environment-friendly, locally available, less inflammable compared to petroleum diesel and does not add GHGs to the atmosphere owing to its closed carbon cycle. However, there are a few drawbacks associated with the use of biodiesel, including, low heating value which results in cold start problems in cold regions, high viscosity which causes poor fuel atomization and difficulty in fuel pumping leading to increased fuel consumption and clogging of some engine parts such as fuel filters and fuel lines thus calling for their replacement quite often. Biodiesel, therefore, generally displays inferior combustion and performance characteristics compared to fossils diesel and as such cannot be used directly in diesel engines. These drawbacks can be mitigated by addition of organic nanoparticles to the biodiesel to improve its combustion. Previous studies have shown that petroleum diesel and biodiesel drawbacks can be mitigated using NPs doped in diesel-biodiesel fuel blends from various feedstocks. However, none, according to the authors' knowledge, has investigated the impact of GNP additives doped in Oleander-Croton biodiesel, thus, this study has attempted to provide insight on the performance and

emission characteristics of a diesel engine operated on a blend of diesel and biodiesel derived from Oleander and Croton oils enriched with GNPs at 50 ppm, 75 ppm, and 100 ppm concentrations, and a comparative analysis carried out on the fuel blends.

1.3 Objectives of the Study

1.3.1 Main Objective

The main objective of this study was to assess the performance and emissions from a diesel engine operated on Oleander and Croton biodiesel blends enhanced with graphene nanoparticles additives.

1.3.2 Specific objectives

1. To determine the proportions of graphene nanoparticles in ppm that give optimum engine performance.
2. To determine the proportions of graphene nanoparticles in ppm that give minimum exhaust emissions.
3. To compare physicochemical properties of the nano-enhanced biodiesel with the existing standards.

1.4 Justification of the Study

Diesel engines emit toxic gases such as UHC, CO and NOx and $PM_{2.5}$ among others which are hazardous to the environment. Diesel-fueled vehicles contribute significantly to these pollutants which are directly and indirectly harmful to human health. The black smoke (soot) from diesel engines is a part of outdoor air pollution contributed mainly by heavy commercial vehicles such as buses and trucks. Long-term exposure to these pollutants contribute to increased risk of illness and death from ischemic heart disease, stroke, lung cancer, lower-respiratory infections (e.g. pneumonia), chronic obstructive pulmonary disease (COPD), type 2 diabetes, among others (Hougaard *et al.,* 2015). A severe problem related to diesel emissions is the presence of polycyclic aromatic hydrocarbons (PAHs) which are known to be mutagenic and/or highly carcinogenic towards humans (Dandajeh *et al.,* 2021).

Carbon monoxide is a serious pollutant in smog mostly emitted by motor vehicles, and can build up to dangerous levels in areas with heavy congested traffic in the capitals and major cities. CO, when inhaled, binds to hemoglobin in the blood, reducing the ability of blood to carry oxygen, thus depriving heart, lungs, brain and other vital organs of oxygen which causes unconsciousness, fatigue, dizziness, impaired judgment, and in some instances can lead to death (USEPA, 2016). It poses a serious threat to people with heart disease because of the fragile condition of the circulatory system and to fetuses owing to the oxygen needs of the developing brain.

Air pollution accounts for 20% of newborn deaths worldwide, most related to complications of low birth weight and preterm birth. In 2019, air pollution contributed to nearly 500,000 deaths among infants in their first month of life (State of Global Air, 2020). Ground ozone exposure has been shown to be responsible for asthma attacks and even death, while sulfur dioxide and nitrogen dioxide can cause respiratory diseases such as lung inflammation and reduced lung function (WHO, 2018). Epidemiological studies show that a lot of deaths and large sums of money is lost in medical costs and lost productivity every year in third world countries as a result of air pollution. These losses, and the associated degradation in quality of life, impose a significant burden on people in all sectors of society, especially the low-income earners.

CO_2 on the other hand is the largest contributor to the greenhouse effect which eventually leads to global warming that results in climate change, whose consequences include: erratic rainfall, flooding, droughts, destruction of coastal areas, reduction in ecosystems diversity and negative impacts on human health.

Owing to the highlighted health and environmental impacts, there is need of reducing the emissions emanating from the use of fossils diesel. Biodiesel serves as the preferred replacement for fossils fuels owing to its low emission characteristics, it is renewable, readily and locally available, biodegradable, besides, its physiochemical properties compare well to those of fossils diesel. In addition, it ensures no CO_2 is retained in the atmosphere, owing to its closed carbon cycle. Thus it aids greatly in mitigating global warming. Biodiesel enhances environmental protection, besides creation of massive

job opportunities since cultivation and processing of the biodiesel feedstocks require human resource input. Construction of biodiesel plants will improve the local economy and social amenities such as schools, hospitals and infrastructure. The presence of large tracts of semi-arid land in the country offers an opportunity for growing crops that are drought resistant such as Oleander, Croton, Castor, Jatropha etc. leading to an improvement of the existing forest cover and thus mitigating against the adverse effects of deforestation, as well as serving as carbon sink. The use of marginal land ensures that the highly productive land is not used for energy production, thereby guarding against competition between biofuels and food production. Besides, biodiesel will foster diversity of energy mix.

However, biodiesel, if applied to CI engine in its pure form performs dismally. This study therefore seeks to enhance the performance and reduce emissions of Oleander and Croton biodiesel fuelled CI engine by doping the biodiesel blend with GNPs, as an attempt to investigate biodiesel from new and varied feed stocks.

1.5 Research Questions

i. Does adding GNPs to Oleander and Croton biodiesel-Diesel blend improve performance and emission characteristics of CI engines?
ii. What quantity of graphene nanoparticles doped in the Oleander and Croton biodiesel-diesel mixture gives optimum engine performance and minimum exhaust emissions?
iii. How do properties of graphene-nano enhanced Oleander and Croton biodiesel compare with those of existing standards?

1.6 Scope of the Study

The study focused on formulating and conducting experiments with the aim of investigating nano-enhancement of biodiesel blend from two local oil crops; Oleander and Croton blended with fossils diesel, using graphene nanoparticles. Oleander and Croton biodiesels as well as fossil diesel were obtained locally while graphene was sourced from NanoShel Company-India. Physico-chemical properties of the biodiesels were determined through experimental analysis. The methodology is outlined in

chapter three and was conducted according to the current best practices. The experiments were carried out at the Mechanical engineering laboratory at Jomo Kenyatta University of Agriculture and Technology (JKUAT) and the data obtained from the experiments analyzed according to the outlined objectives of this study. Performance and emission characteristics of the engine at various dosing levels of nanoparticles was analyzed. The study did not include transesterification of the oils.

CHAPTER TWO

LITERATURE REVIEW

2.1 Introduction

This chapter presents a review of literature related to the objectives of the study in order to provide an empirical framework on the problem area. The information obtained from the literature was applied in developing the methodology of the study.

2.2 Theoretical background

Biodiesel is a renewable, biodegradable and environment-friendly alternative fuel to fossil diesel that can fulfil energy security needs without compromising the engine performance. It is derived from renewable sources such as vegetable oils, animal fats and used cooking oil through transesterification process, which entails addition of a short-chain alcohol typically methanol or ethanol to the oil under mild heat conditions in the presence of a base catalyst such as Potassium hydroxide (KOH) and Sodium hydroxide (NaOH), with glycerine as the by-product, i.e. oil + alcohol → biodiesel + glycerol (Elgharbawy *et al.,* 2021). The transesterification reaction is shown in equation (2.1) (Mujeeb *et al*., 2016), and the schematic of the biodiesel production in Figure 2.1.

$$\begin{array}{l} CH_2OCO \\ R_1 \\ \quad | \\ CHOCO \\ R_2 \\ \quad | \\ CH_2OCO \\ R_3 \end{array} + 3CH_3OH \quad \underset{\rightleftarrows}{NaOH} \quad \begin{array}{l} CH_2OH \\ | \\ CHOH \\ | \\ CH_2OH \end{array} + \begin{array}{l} CH_3COOR_1 \\ | \\ CH_3COOR_2 \\ | \\ CH_3COOR_3 \end{array} \qquad (2.1)$$

Triglyceride Methanol Glycerol Biodiesel

R_1, R_2, and R_3 represent hydrocarbon chain of the fatty acid.

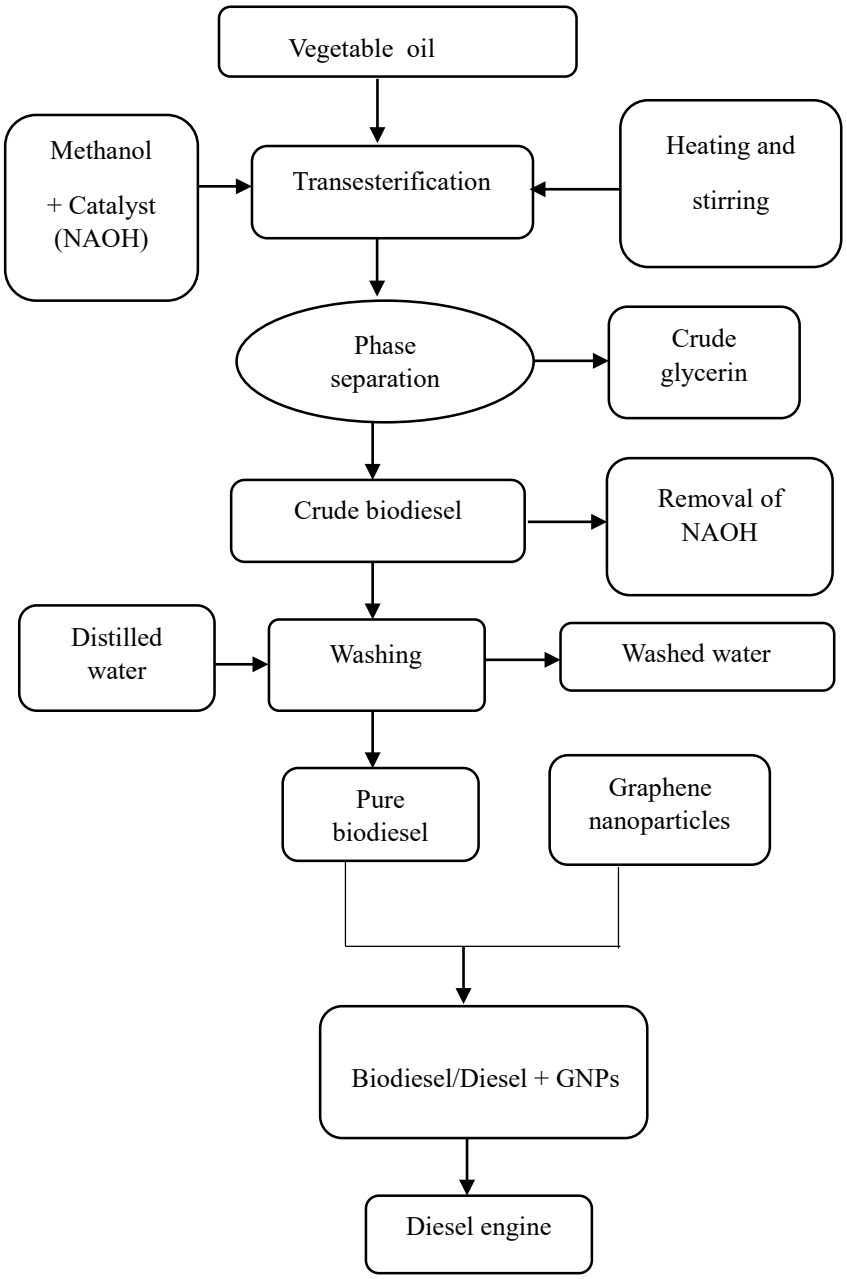

Figure 2.1: Schematic of biodiesel production and fuel blends preparation process

Source: (Mallikarjuna *et al.,* 2022; Ruhul *et al.,* 2015)

However, the biodiesel produced has a higher viscosity compared to the fossil diesel owing to its molecular structure which comprises of long chain of carbon atoms with hydrogen atoms attached, and an ester functional group at the end, unlike that of fossil diesel which has no ester group (Pham, 2015). As such biodiesel cannot be used

directly in conventional diesel engines. The average chemical formula for fossil diesel is $C_{12}H_{23}$ while that of biodiesel is $C_{17}H_{34}O_2$, with the ester group $–CO_2CH_3$ at the end of the long carbon chain. Figure 2.2 shows the molecular structure of (a) biodiesel and (b) Petroleum diesel.

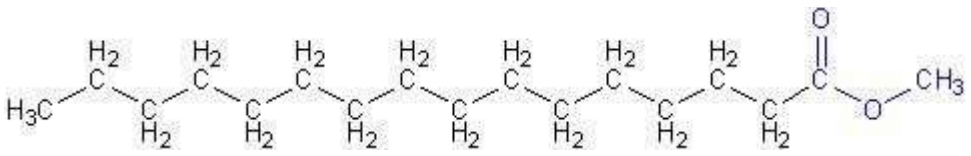

(a)

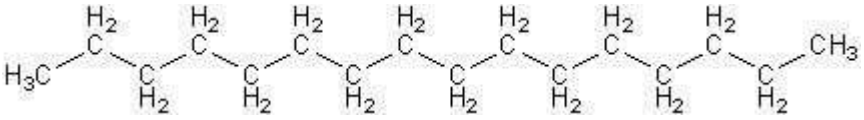

(b)

Figure 2.2: Molecular structure of (a) biodiesel and (b) Petroleum diesel

Source: (Masera & Hossain, 2017)

Biodiesel has additional oxygen which reacts with nitrogen in the atmosphere to form NOx as shown in equations (2.2), (2.3) and (2.4), thus biodiesel emits higher quantities of NOx compared to fossil diesel.

$$N + O_2 \leftrightarrow NO + O \quad \text{.....(2.2)}$$

$$N_2 + O \leftrightarrow NO + N \quad \text{.....(2.3)}$$

$$N + OH \leftrightarrow NO + H \quad \text{.....(2.4)}$$

2.3 Biodiesel Feed Stocks

The feed stocks for biodiesel include:

2.3.1 Jatropha (Jatropha curcas)

Jatropha is a multi-purpose, shrubby tree belonging to the Euphorbiaceae family. It is 3 m -5 m high under normal conditions, and as much as 8 m - 10 m under favorable

conditions. It grows in tropical and sub-tropical climates across the developing world. In Kenya, Jatropha is mainly grown in Naivasha, Kitui, Nakuru, Marakwet, Nyanza, coastal regions and in Meru. Jatropha oil is colorless immediately after extraction and pale yellow after storage, it is liquid at room temperature. Among the seed oil producing plants, Jatropha is preferred for biodiesel production because it has a relatively high oil content that ranges from 38.7% to 45.8% (Jonas, Ketlogetswe & Gandure 2020) is non-edible and therefore does not compromise food security as is the case with food crops such as palm and soybean. It is drought resistant, thus does not compete with land suitable for food production(Vaknin, Yermiyahu, Bar-Tal, & Samocha, 2018). Jatropha oil burns with a clear smokeless flame and pests and diseases do not pose a significant threat to the plant due to the insecticidal and toxic characteristics of all parts of the plant (Ubulom, Yaro, & Udoh, 2021) Besides, the physiochemical properties of jatropha biodiesel such as, flash point, density, acid value, iodine value, calorific value, saponification value and kinematic viscosity are within the range of the standard biodiesel thus Jatropha oil is suitable for biodiesel production (Ahmed, Giwa, Ibrahim, & Giwa 2016). However, jatropha is not a commercially viable feedstock for biodiesel production owing to the low seed yield (Muskens, 2014), high FFA content 2.23% which requires application of two-stage process (esterification and then transesterification) (Silitonga, Ong, Mahlia, Masjuki & Chong,2014), besides, it is labor intensive and is associated with fungal infections in infants (Doughari & Abraham, 2021).

2.3.2 Palm (Elaeis guineensis)

Palm tree is a plant native to Africa, from which palm oil, an edible vegetable oil is derived. It is widely used as a cooking oil. Palm oil has high biodiesel production yield, high flashpoint, good oxidation stability and an acceptable saponification ratio, cetane number and iodine value. Biodiesel obtained from palm oil reduces harmful emissions significantly from an unmodified diesel engine (Appavu, Madhavan, Jayaraman & Venu 2019). Combustion of palm oil biofuel does not increase the level of CO_2 in the atmosphere as the oil is merely returning carbon dioxide obtained earlier from the atmosphere through photosynthesis, as such, the biofuel is regarded as carbon neutral. However, palm oil use as a biodiesel feedstock may not be sustainable considering it

is edible and therefore could compromise food security (Issariyakul & Dalai, 2014). Moreover, it has a high viscosity and as such cannot be used alone, it has to be blended with the conventional diesel. Additionally, it has a high freezing point thus may become solid at low temperatures though it may perform satisfactorily in hot climates.

2.3.3 Castor (Ricinus comminis)

Castor is a perennial shrub from the Euphorbiaceae family with green, reddish to purple stems and finger-like leaves that originated in Ethiopia. Castor can reach up to 9 m in the wild, but cultivated varieties generally grow to between 1 m – 4 m. It is a non-edible biodiesel feedstock with a strong adaptation to different climatic conditions and can grow in marginal soils, thus it does not compromise food security. Castor oil is liquid at room temperature, light yellow, and slightly pungent. Recently, the use of castor oil has attracted attention as a biodiesel feedstock due to its high oil content, (one bean oil content is 45.7% to 54%), high miscibility in alcohol, low reaction temperature, low iodine content, low freezing point, high ricin oleic fatty acid which aids in the transesterification process hence low production costs (Román-Figueroa Cea, Paneque & González 2020). Furthermore, biodiesel from castor oil is biodegradable, non-toxic, renewable, low GHG emission, high flash point, and similar energy content to fossil diesel (Osorio-González, Gómez-Falcon, Sandoval-Salas, Saini, Brar & Ramírez 2020). However, castor has a relatively low seed yield, approximately 450 kg/ha compared to that of other biodiesel feedstocks, such as Yellow oleander which is 1575 kg/ha. Besides, the biodiesel has a high viscosity and high water content which could potentially damage internal combustion engines, (Keera, El Sabagh & Taman, 2018)

2.3.4 Yellow Oleander (Thevetia peruviana)

Yellow Oleander which is proposed for this study is also called ‘be still tree’, lucky nut, yellow bell among other names is a small ornamental tree that grows to about 1.5 m - 2.3 m high with leaves about 130 mm -150 mm in length and bright yellow funnel-shaped flowers bearing slightly fleshy globelike fruits 40 mm -50 mm in diameter, green, and black upon ripening, with each fruit producing two seeds (Rojas-Sandoval, 2022). Yellow oleander tree is largely grown in North-East India and is widespread in

American, Asian and African continents (Bora, Gogoi, Deka, & Kakati 2014). *Thevetia peruviana* is used traditionally to treat, among others, malarial fever, headaches, hemorrhoids, constipation, skin disorders, jaundice and snake bites (Ahmad,, Hamid, Sharma, & Bhardwaj 2017).

In Kenya it is largely grown in Makueni, Tana River, Siaya, Homabay and Kajiado counties. Its local names are *Kamulla* in Kamba dialect and *chamama* in Luo where it flourishes quite well as an ornamental plant. It is drought-tolerant once established but responds well to occasional deep watering, and can grow in a broad range of soils, it is non-edible and not labour intensive. The seeds, if processed healthy can be used as an alternative protein source in animal feed formulation. The oil could also be useful in the production of oleo chemicals such as liquid soap, shampoos and paints (Basumatary, Nath, Kalita, Das & Basumatary 2020).

Thevetia peruviana is suitable for use as a biodiesel feedstock considering it is non-edible and drought resistant implying it can flourish well in arid and semi-arid areas where there are large tracts of idle land, thus it does not compete with land used for food production, is not a threat to food security, does not call for cutting of any trees and therefore its cultivation does not interfere with the ecosystem and also is environment friendly as no harmful gases, especially GHG such as CO_2, methane and nitrous oxide are released to the environment as is often the case when change in land use is involved (UNCCC, 2023). Besides, the trees will act as carbon sink. 3000 saplings can be planted in a hectare of non-arable land, out of which 52.5 tons of seeds (3500 kg of kernel) can be collected. This can translate to a seed yield of 52.5 tons/ha and about 1750 litres of oil (Basumatary, 2014). The Seeds obtained from the oleander tree are crushed using a mechanical expeller for oil extraction.

Yarkasuwa *et al.,* (2013) investigated the suitability of Yellow Oleander oil for biodiesel production and observed that; Yellow oleander seeds have a high oil content of 67% and a biodiesel yield of 91.6%, thus can be harvested for large scale production of biodiesel, a flash point of 198 ^oC which is higher than that of petroleum diesel which is approximately 60 ^oC hence its tendency to cause fire hazards is low and thus safe to handle. The density of YOME is 0.866 g/cm^3 which conforms to the EN 14214

standards of 0.860- 0.900 g/cm^3 and also compares well with that of petroleum diesel which is 0.850 g/cm^3 as per ASTM D975 Standards, while the pour point (the lowest temperature at which the fuel ceases to flow due to high viscosity) is -2 ºC which falls within the recommended range for biodiesel which is -15 ºC to 10 ºC and -35 ºC to 15 ºC for conventional diesel as per ASTM D6751 and ASTM D971 standards, respectively. They also established that YOME's biodegradability is 86.2% which is higher compared to that of petroleum diesel's 26.82%, thus it is environment-friendly. The moisture content of the oil was 2.2% which implies that the oil can be stored for long and still maintain its original quality.

Basumatary, (2014) trans esterified yellow oleander seed oil and reported 95wt.% yield of biodiesel achieved at room temperature (32 °C) in 3 hours. They also found that each seed of yellow oleander contained 60-65% oil content. Yellow Oleander oil has a free fatty acid (FFA) value of 0.63% which is the value ideal for transesterification to take place (Dallatu, Agbaji & Ajibola 2018). FFA value of more than 1% leads to formation of soap which complicates biodiesel recovery and compromises its quality. The cetane number for YOME is 48 (Dallatu *et al.,* 2018) which compares well to that of petroleum diesel which is between 45 and 55.

Rupasianghe & Gunathilaka, (2018) trans esterified yellow oleander seed oil and observed the following physiochemical properties: The density of YOME was 887 kg/m^3 which agreed with EN 14214 standards of 860 kg/m^3 to 900 kg/m^3, and compared well with that of fossil diesel which is 816- 840 kg/m^3, kinematic Viscosity @ 40 ºC was 5.96 mm^2/s which conformed to the ASTM D 6751 standard which is 1.6 - 6.0 mm/s^2 and a gross calorific value of 37.74 MJ/kg which agreed with the EN 14213 standards for biodiesel which is 33-40 MJ/kg.

Figure 2.2 (a), (b), (c) and (d) shows oleander tree, oleander fruits, dried nuts and deshelled nuts respectively.

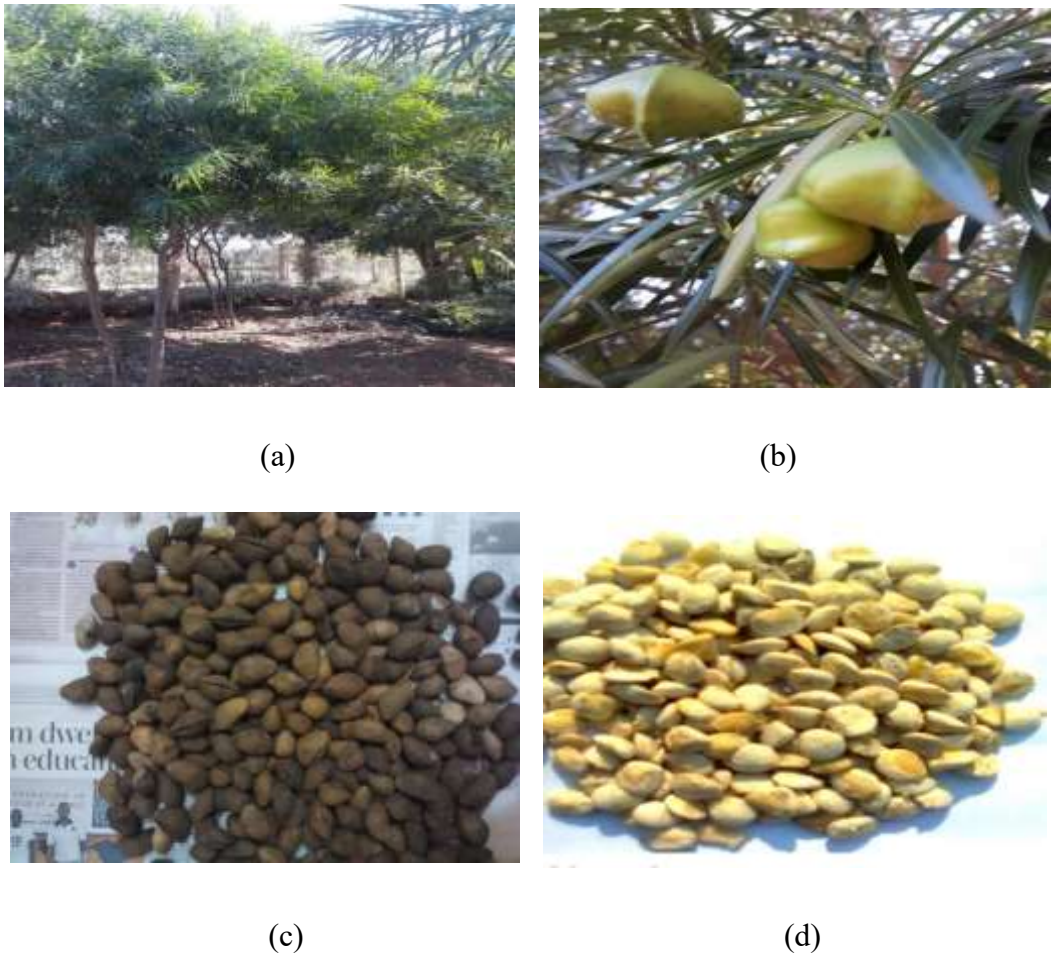

(a) (b)

(c) (d)

Figure 2.3: Yellow Oleander (a) Tree (b) Fresh fruits (c) Dried nuts (d) De-shelled nuts (Mtito Andei, Kenya in May 2022)

2.3.5 Croton (Croton megalocarpus)

Croton, proposed for this study is a widespread indigenous tree commonly found in sub-Saharan Africa including Kenya, Tanzania, Rwanda, Burundi, Zimbabwe, Malawi, Uganda, Zambia, Democratic Republic of Congo and Mozambique. The local names for the tree are; *Mukinduri* in Kikuyu, Embu and Meru dialects; *Msenefu* in Swahili, *Omkinduli* in Luhya, *Kelelwet* in Kipsigis and *Muthulu* in Kamba. Croton is widespread throughout a wide range of biophysical limits. In Kenya it flowers at the end of April and early May. After pollination by bees, fruit development takes several months, producing mature seeds in October through December in central and northern Kenya, and in January through February in western Kenya. Croton tree is commonly found in forests and rural farms where it is used to mark boundaries. It grows up to 36

meters high, maturing after 5-7 years. The tree is drought resistant, not labour intensive and is not browsed by animals. Its upper side has a dominant canopy-like flat crown with pale brown or dark grey oval shaped leaves which are green on the upper surface and pale underside. Croton trees, upon maturity yield nuts containing three non-edible seeds, dark in colour. Its seeds are used to treat and manage diseases such as gallbladder problems, coughs, colds, wounds, blocked intestines, malaria and also to cleanse the stomach and intestines (Maroyi, 2017). Croton nuts are a good source of income to the rural community; harvest time can last up to six months a year, making it a steady source of income. Furthermore, the trees don't require any use of fertilizer thus it is cheap to cultivate and the returns are enormous (Secorun, 2017). Besides, the seeds are used as poultry feed, owing to their high protein content (Ombaka, Gachuiri & Abong, 2019). Croton has a huge potential to reclaim eroded soils and restore them to productivity. Leaves from the croton trees have greatly improved the fertility and soil texture in the regions where they are grown while providing cover that helps in reducing evaporation during the rainy season, moreover, Croton husks can be used as a soil conditioner.

Recently, Croton was identified as a biodiesel resource owing to its non-edibility local availability as well as its remarkable cold flow properties that has rendered it useful in cold regions. Moreover, the properties of croton biodiesel meet the minimum requirements of both the ASTM D6751 and EN- 14214 biodiesel standards. Osawa *et al.,* (2014) experimented biodiesel from croton oil and from the experiment, the Density, Kinematic viscosity, Calorific value, Cloud point, Pour point and Flash point were found to be, 0.8858 g/cm^3, 4.51 mm^2 /s, 39179 J/kg, -1.5 ^oC, -6.5 ^oC, and >200 ^oC, respectively, which compared well to those of fossils diesel which were 0.8231 g/cm^3, 2.87 mm^2 /s, 44648 J/kg, 4.0 ^oC -2.0 ^oC, and 65 ^oC, respectively. The pour and cloud points of croton biodiesel were lower compared to those of fossil diesel which rendered it more suitable for operation in cold regions. The flash point for CMO (>200 ^oC) obtained conformed to the ASTM recommended value of 130 ^oC (Minimum), thus its tendencies to cause any fire hazard are low. Figure 2.3 (a), (b), (c) and (d) shows croton tree, croton fruits, dried croton nuts and deshelled croton nuts, respectively.

(a)

(b)

(c)

(d)

Figure 2.4: (a) Croton Tree (b) Croton fruits (c) Dried Croton nuts (d) Deshelled Croton nuts. (Makindu Kenya, May 2022)

2.4 Biodiesel Nano additives

Fuel nano additives are metal-based, organic based or carbon-based substances which are easily soluble in fuel. Their main purpose is to provide or improve beneficial characteristics of the fuel without compromising performance and combustion parameters, owing to their impressive attributes such as larger surface area, good

catalytic properties, rapid oxidation and better stability (Praveena, Venkatesan & Gupta, 2018).

They are broadly classified as refinery products, distribution system products and automotive performance enhancement products. They are further subdivided into antioxidants, cetane improvers, anti-knocking agents, anti-freezing agents, stability improvers, ant-corrosion additives, cold flow improvers, fuel borne catalysts, and anti-wear agents. After several studies, researchers have found that modification of fuel with respect to its physicochemical properties yields better results in enhancing the engine performance and controlling the exhaust emissions rather than carrying out engine modifications (Venkatesan *et al.,* 2017).

2.4.1 Metal-based nano-additives

Combustion characteristics of fuel can be improved by addition of metals and metal oxides to the fuel in the range of micro or nano sizes through parts per million (ppm) or percentage by weight ratios (Venkatesan *et al.,* 2017). Metals like iron (Fe), aluminum (Al), magnesium (Mg) manganese (Mn), silver (Ag), gold (Au), copper (Cu), boron (B), etc. and metal oxides such as zinc oxide (ZnO) (Nanthagopal, Ashok, Tamilarasu, Johny & Mohan, 2017),copper oxide (CuO) (Channappagoudra, 2021) etc. are used as additives to improve the fuel physicochemical properties.

Metal-based nano-additives have the potential to reduce exhaust emissions and improve fuel efficiency, however, they may cause environmental and health concerns if they find their way to the environment (Bhardwaj, Shukla, Maurya, Singh, Uttam & Gopal, 2017). A significant accumulation of ZnO NPs can damage the DNA of organisms (Attia, Nounou & Shalaby, 2018)

From the foregoing review, it is clear that using metal-based nano additives for biodiesel enhancement will have a severe impact on human health and the environment.

2.4.2 Organic nano-additives

These are biologically derived or biomass based nano additives synthesized from living organisms such as plants, algae, fungi, and bacteria. They are mainly used as CI engine combustion enhancers owing to their high oxygen content and are commonly referred to as oxygenated additives. They include Ethanol, n-Butanol, Diethyl Ether and Methanol (Madiwale Karthikeyan, & Bhojwani, 2017). They possess high volatility and high cetane index. However, they have a low heating value compared to that of conventional diesel thus incompatible with cold weather conditions.

2.4.3 Carbon-based nano-additives

These are nano-additives derived from carbon including Graphene nanoparticles, single-wall carbon nanotubes (SWCNT), multi-wall carbon nanotubes (MWCNT) and Graphene oxide nanoparticles. They are environment-friendly biodiesel fuel additives since they are devoid of any metal components, with a host of desirable chemical, physical, mechanical, and electrical characteristics hence the reason they are proposed for this study. These additives possess interesting properties such as high surface area and excellent thermal conductivity, which makes them preferred candidates for biodiesel nano-additives (Daud *et al.,* 2022). Carbon-based NPs are classified as energetic NPs. Energetic NPs take part as reactants in exothermic reactions which increases the total released energy (Sisim *et al.,* 2020) which eventually increases the calorific value of the fuel (Basha & Anand, 2014). Carbon-based nano-additives form a long-term stable dispersion in the base fuels with minimal particle agglomeration compared to metallic additives, thus do not necessarily require use of a surfactant (Elsaid, Abdelkareem, Maghrabie, Sayed, Wilberforce, Baroutaji & Olabi, 2021). Being energetic NPs, they are combustible and therefore do not form any deposits in the CI engines unlike Metal based NPs which deposit on the engine walls and in the exhaust system and as such cannot be used in CI engines for long. The NPs are converted to CO_2 during combustion and exit with the exhaust gases, unlike metallic NPs which are emitted to the environment thereby causing environmental pollution. This reaction may result in a slight increase in CO_2 emission. The increment, however, is very minimal such that it is overridden by the significant decrease in CO emissions

(Debbarma, Misra & Das, 2020), furthermore, it is absorbed by plants and used for photosynthesis, thus does not contribute to global warming (Hanaki & Portugal-Pereira, 2018).

2.5 Nano fluids

Nano fluids are fluids comprising of micro-sized particles ranging from 1 nm to 100 nm in size doped inside the base fluid (BF), usually diesel/biodiesel. Addition of NPs improves fuel properties such as caloric value, cetane number, flash point, density and kinematic viscosity which enhances combustion. Additionally, NFs possess high surface to volume ratio and high thermal conductivity which improves performance of the CI engine as well as reducing exhaust emissions (Yusof, Sidik, Asako, Japar, Mohamed, & Muhammad 2021). Other special qualities of NFs include, better stability than other colloids, better lubrication of the engine parts, reduction of erosion and clogging in micro channels and reduction in pumping power (Mukherjee & Paria, 2013). Increasing the quantity of NPs can reduce emissions significantly and enhance engine performance, however, excessive number of NPs will lead to incomplete combustion owing to the increased viscosity (Yusof *et al.,* 2021).

NFs are divided into two types: Metallic NFs and non-metallic NFs. Metallic NFs are prepared by doping metallic additives in the BF while non-metallic NFs are prepared by doping non-metallic additives in the BF. Preparation technique of NF is very crucial as it affects the properties and stability of the resulting NF significantly. There are 2 primary methods for preparation of NFs: 1 step method, which entails creating the BF and NPs together, and the 2-step process which involves mixing the BF with commercially acquired NPs and then stirring using an ultrasonic vibrator or higher shear mixing device. The stirring or ultra-sonication should be done frequently to reduce particle agglomeration. Ultrasonic vibration breaks up cluster formation of NPs and helps to scatter the nanostructures within BF. The main advantages of the one-step method are uniform dispersion of NPs in BF, hence enhanced stability and minimized agglomeration of NPs. This is mainly because NPs are directly formed in the BF therefore transportation and storage of NPs is avoided. On the other hand, the one-step method is limited to certain NPs and BF and their specific combination. Additionally,

the method results in limited NF quantity and NPs concentration, and is costly too. The 2-step process is the most preferred method because of the possibility of acquiring commercially readily available NPs with given specification and known characterization, hence reduces the time required for exhaustive NPs preparation methods which is followed by advanced characterization techniques that is not only expensive and time consuming, but also exhaustive. However, it requires very well dispersion followed by vigorous stirring to avoid agglomeration and aggregation of the NPs in the BF. To increase the stability of NFs, diverse techniques have been employed, such as extended ultra-sonication, addition of surfactants as well as PH control. Ultrasonication technique facilitates disintegration of possibly agglomerated NPs back to nanometre range (Sandhya Ramasamy, Sudhakar, Kadirgama & Harun, 2021).

This study seeks to use the 2-step process owing to the highlighted advantages. It also proposes to use graphene-based NFs as opposed to other NFs reasons being; Graphene NF is easy to synthesize, has a higher heat conductivity (Mehrali, Sadeghinezhad, Latibari, Kazi, Mehrali, Zubir & Metselaar, 2014), lower demand for pumping power and a longer suspension stability over other NPs owing to the light weight and low density of the GNPs (Le Ba, Mahian, Wongwises & Szilágyi, 2020). Moreover, it has enhanced chemical reactivity owing to the large surface area/volume ratio, better lubrication (Mujtaba *et al.,* 2020) and lastly reduced erosion, corrosion and clogging in systems (Suneetha & Reddy, 2016). In addition, graphene-based NF possesses slightly lower viscosity at higher temperatures compared to other NFs (Hamze, Cabaleiro, & Estellé 2021).

2.6 Graphene Nanoparticles

Graphene, the nano additive proposed for this study, is an allotrope of carbon in the form of a 2D single layer of carbon atoms that are tightly bonded to each other in a hexagonal lattice (Tiwari Sahoo, Wang & Huczko, 2020). It is the basic structural element of other carbon allotropes, including 3D graphite, charcoal, 1D carbon nanotubes (CNTs) and 0D fullerenes. It is produced by isolating one-layer thickness from graphite through various techniques such as chemical vapor deposition (CVD),

exfoliation, chemical synthesis and pyrolysis. Exfoliation method is the most preferred method as it yields superior, defect-free, few-layered graphene with a larger surface area (Abbasi, Akbarzadeh, Kouhi, & Milani, 2016; Moosa & Abed, 2021).

Graphene, the thinnest material ever known to man, only one carbon atom thick has attracted a lot of attention from researchers in several fields, including its use in biodiesel blends to improve diesel engine performance and emission characteristics owing to its astonishing properties, such as high surface area-to-volume ratio of about 2600 m^2/g (Gadipelli & Guo, 2015), which is arguably the largest of all 2D crystalline-layered materials (Igor Ivanov, 2019). Being single-atom thick, all the atoms are exposed at the surface and therefore provide a wide surface for the particle-to-fuel interaction, which enhances chemical reactivity as well as thermal transfer from the NPs to the host fuel, thereby reducing the ignition delay (ID). Moreover, graphene possesses an exceptionally high thermal conductivity of up to 5000 W/mK which is 10 times higher than that of copper (401 W/mK), (Mbayachi *et al.,* 2021), which increases the calorific value of the base fuel and hence increases the evaporation rate, which leads to enhanced combustion that results in improved fuel economy.

The excellent friction and wear reduction properties of graphene makes it a promising material for tribological applications (Masood *et al.,* 2017; Zhai *et al.,* 2017). Furthermore, the small particle sizes that are tightly packed in the crystal lattice, coupled with the weak Vander Waals forces between the GNP atoms reduces the possibility of fuel agglomerating, thus enhancing the formation of a homogenous mixture with the host fuel (Song *et al.,* 2015; Yang *et al.,* 2015). Graphene has an extraordinary electron conductivity of 106 S/m, which is 140 times greater than that of silicon. This is attributed to the two pi-electrons that are present in every hexagon of the graphene sheets, which donate an extra electron to π the bond. These pi-electrons are delocalized at room temperature, thereby yielding high conductivity (Bolotin *et al.,* 2008).

GNPs are preferred over other carbon-based nano additives such as graphene oxide and MWCT because of their high C.V., superior engine performance and low emissions (EL-Seesy & Hassan, 2019; Jeyaseelan & Chako, 2020). The doped GNPs

are converted to CO_2 during combustion, unlike metal-based NPs which are emitted directly from the exhaust to the environment, causing environmental pollution. Because GNPs is entirely oxidized in high-temperature combustion zones with virtually no additional residues other than common combustion products, it can be viewed as a fuel supplement, contributing towards energy density and also as environment-friendly (Chehroudi, 2016), hence the more the reason it is the preferred candidate for this study.

2.7 Summary of Related Literature

Research on the performance and emission characteristics of the CI engine running on biodiesel from various feed stocks enhanced with nanoparticles has previously been conducted and the results compared with those of fossils diesel.

Debbarma *et al.,* (2020) doped palm biodiesel-30% blended with diesel-70%, with GNPs at mass fractions of 50, 75 and 100 mg/L. They observed that the inclusion of GNPs resulted in 2.5% increase in BTE, 17% and 34% reduction in UHC and CO emissions, respectively, and 3.8% increase in NOx emission. Similarly EL-Seesy *et al.,* (2018) mixed graphene nanoplatelets (GNPs) at 25, 50, 75 and 100 ppm on a mixture of 80% neat diesel and 20% Jatropha biodiesel. The results revealed a rise of 25% in BTE and a 20% reduction in BSFC relative to the neat biodiesel at 50-75 ppm dosing level. On the other hand, UHC, NOx and CO emissions decreased by 50%, 40%, and 60%, respectively, at 25–50 ppm concentration. Optimal engine performance and lowest emissions were realized at 50 ppm dosage. Razzaq *et al.,* (2021) experimented the effect of GONPs and DMC10 additives doped in palm biodiesel-30% and diesel-80% mixture at 40, 80 and 120 mg/L concentrations, on the performance and emissions of CI engine. They recorded a 22.80% increase in BTE, 3.65% and 5.05% reduction in NOx and BSFC, respectively, for the 40 ppm concentration and a 25% and 4.41% reduction in HC and CO, respectively, for the un-doped fuel relative to all tested samples.

Mallikarjuna Rao, Janga, Dhana Raju, & Arifa, (2022) demonstrated that inclusion of GNPs to JME -20% and diesel - 80% (JME20), at concentrations of 25, 50, 75 and 100 ppm improves performance characteristics significantly, especially at 50 ppm

concentration. NOx, CO, HC emissions and smoke are reduced significantly for the nano- enhanced blends compared to JME20. El-seesy, Attia and El-batsh (2018) conducted an experimental investigation to establish what proportion of alumina nanoparticles ranging from 10 ppm to 50 ppm blended with 20% Jojoba methyl ester and 80% diesel yielded optimal engine performance with minimum exhaust emissions. The results revealed that minimum emissions were achieved at 20 ppm dosing level, where CO, UHC and NOx were reduced by 80%, 60% and 70%, respectively. On the other hand, optimal engine performance was attained at 40 ppm, with BSFC reducing by 12%. After critically comparing the engine performance and emissions at different concentration of alumina nanoparticles in the biodiesel blend, they concluded that remarkable engine performance parameters is achieved at 30 ppm dosing level.

Soudagar *et al.,* (2020) investigated combustion, performance and emission characteristics of common rail direct injection engine operated on different fuel blends which included neat diesel (D100), neat diesel doped with 30 ppm of zinc Oxide (ZnO) nanoparticles (D10030), 80% of neat diesel blended with 20% of Mahua oil methyl ester (MOME20) and MOME20 doped with 30 ppm ZnO. The results revealed a reduction of BSFC, smoke, CO, UHC and NOx by 10.9%, 18.2%, 12.6%, 8.4% and 5.74% respectively for the D10030 and 7.7%, 8.6%, 11.5%, 13.1% and 7.79% respectively for the MOME2030 blend. On the other hand, the BTE increased by 9.65% for D10030 and 16.4% for MOME2030 for injection timing (IT), and 8.83% for the D10030 and 5.06% for MOME2030 for the injection opening pressure (IOP). The heat release rate and cylinder pressure for MOME2030 and D10030 increased by 12.28% and 7.35%, and 17.1% and 6.8%.

Bhagwat, Pawar & Banapurmath, (2015) doped HOME with GNPs at 25 ppm and 50 ppm concentrations. They observed that doping the fuel with GNPs increased BTE and decreased UHC, CO, and NOx emissions relative to HOME. Optimal performance and minimum emission characteristics were achieved at 50 ppm concentration. Likewise, Nair, Prasad, Kumar, Thakur, Samhita, & Aravinda (2021) added GNPs to a mixture of 80% diesel and 20% *Karanja* biodiesel at 25, 50 and 75 ppm. From the results obtained, the performance and emission characteristics of the nanoparticle-enhanced fuel were comparable to those of petroleum diesel. BTE for the nanoparticle-enhanced

fuel increased significantly while BSFC, NOx and CO emissions reduced relative to *Karanja* biodiesel. The lowest HC emission was achieved at 75 ppm concentration except at zero load where diesel recorded the lowest. Manavendra & Banapurmath, (2017) conducted a study using WCOME doped with GNPs at 20, 40 and 60 mg/L concentrations and reported increased BTE, decreased BSFC and ignition delay, improved calorific value and lower HC and CO in comparison to the biodiesel, while NOx increased slightly.

From the literature review, it can be concluded that diesel-biodiesel blends doped with nanoparticle additives are a promising technique for enhancing engine performance and reducing exhaust emissions. However, most of the feedstocks used are edible and could potentially lead to food insecurity, while others such as jatropha are not commercially viable feedstock for biodiesel production owing to the low seed yield (Muskens, 2014) and high production costs owing to the high free fatty acid (Silitonga *et al.,* 2014). Besides, they are labour intensive and are associated with fungal infections in infants (Doughari & Abraham, 2021). *Honge/Karanja* biodiesel, on the other hand has a higher cloud and pour point which is 6 ºC and 3 ºC, respectively (Nayak *et al.,* 2017) compared to that of croton biodiesel‘s -1.5 ºC and -6.5 ºC, hence unsuitable for application in cold regions. Moreover, some of the nanoparticles used are metal-based, which studies have shown are toxic(Igbokwe *et al.,* 2020) and harmful to the environment (Bhardwaj *et al.,* 2017).

Various researchers have demonstrated that Croton and Oleander oils can be used for biodiesel production owing to their non-edibility, drought resistance, local availability as well as remarkable physiochemical properties (Dallatu *et al.,* 2018; Osawa *et al.,* 2014). Graphene on the other hand is carbon-based and therefore less toxic and is environment-friendly. Besides its highly attractive properties renders it a desirable candidate for biodiesel enhancement. However, there is scarce literature on the use of graphene nanoparticles with biodiesel from Croton and Oleander oils as fuel for diesel engine. This study therefore aims to investigate the effect of adding GNPs to OCB20 on the single-cylinder, four-stroke CI engine’s performance and exhaust emissions and the most suitable GNPs concentrations for best engine performance and minimum emissions. Table 2.1 depicts the studies by various authors and the gaps in their study.

Table 2.1: Studies by various authors and the gaps in their study

Author	Study	Gap
(Fayad *et al.*, 2022)	Added copper oxide (CuO_2) NPs to rapeseed methyl ester (RME) and diesel blend	CuO-NPs have been shown to induce oxidative stress and inflict damage on mitochondria and lysosomes in human blood lymphocytes (Assadian *et al.*, 2018).
(Hawi *et al.*, 2019)	Iron-doped cerium oxide nanoparticles + WCOME–diesel blend	CeO_2 NPs could negatively impact on male reproductive health (Lee & Park, 2022), and are harmful to plants at higher doses (Prakash *et al.*, 2021)
(D'Silva *et al.*, 2015)	TiO_2 nanoparticles amalgamated in neat diesel	TiO_2 have adverse effects on the male reproductive system Deng *et al.*, 2022)
(Debbarma *et al.*, 2020)	Palm biodiesel-diesel + GNPs	Edible feedstock, posing a threat to food security.
(El-seesy *et al.*, 2018)	Alumina nanoparticles + Jojoba biodiesel-diesel	Inhalation of alumina nanoparticles can cause pneumonia, autism, stroke, cancer (Igbokwe *et al.*, 2020)
(Soudagar *et al.*, 2020)	Diesel- Mahua oil methyl ester + zinc Oxide NPs	Recurrent oral exposure to zinc oxide nanoparticles ZnONPs could be toxic to the neural system(Attia *et al.*, 2018)
(Nair *et al.*, 2021)	Diesel - *Karanja* biodiesel + GNPs	*Honge/Karanja* biodiesel has a higher cloud and pour point (Nayak *et al.*, 2017) thus unsuitable for application
(Mallikarjuna Rao *et al.*, 2022)	Jatropha biodiesel-diesel + GNPs	Jatropha is not commercially viable feedstock for biodiesel production owing to the low seed yield (Muskens, 2014), and high production costs (Silitonga *et al.*, 2014). Besides, it is labour intensive and are associated with fungal infections in infants (Doughari & Abraham, 2021)

CHAPTER THREE

MATERIALS AND METHODS

3.1 Experimental design

Five fuel samples were used for the study including Petroleum diesel denoted by D100, Diesel (80%) blended with 20% of Oleander and Croton biodiesel, denoted by OCB20 and OCB20 doped with GNPs at mass fractions of 50 mg/L (50 ppm), 75 mg/L (75 ppm) and 100 mg/L (100 ppm) denoted by GNP50-OCB20, GNP75-OCB20 and GNP100-OCB20, respectively. The experiments were performed on a single-cylinder four-stroke compression ignition engine.

3.2 Biodiesel and Nanoparticle Supplies

Petroleum diesel, Oleander and Croton biodiesels used in the current study were acquired commercially from local outlets while graphene nanoparticles were sourced from NanoShel Company, India where it was synthesized using exfoliation method, the most preferred as it yields superior, defect-free, few-layered graphene with a larger surface area (Abbasi *et al.,* 2016). The specifications of GNPs are shown in Table 3.1.

Table 3.1: Specifications of the nanoparticles

Description	Graphene nanoparticles
Manufacturer	Nano Shel-India
Carbon content	99.5%
Average particle size	2-4 nm thick, 5 μm wide
Thermal conductivity	3000 W/mK
Appearance	Black
Specific surface area	120-140 m^2/g
Morphology	Flaky
State	Amorphous powder

3.3 Experimental procedures

3.3.1 Preparation of Biodiesel Blends

Oleander and Croton biodiesels were mixed in different proportions in a bid to establish the ratio that would yield a blend with the most desirable characteristics (refer to appendix 2). From the results obtained, a mixture of 70% Oleander biodiesel and 30% Croton biodiesel was arrived at. This blend was denoted by OCB. OCB-20% was blended with petroleum diesel-80% using a magnetic stirrer for about 20 min at 1000 rpm to form OCB20. The 80:20 diesel to biodiesel ratio was preferred because 20% biodiesel blend has the fuel properties such as kinematic viscosity, density and calorific value similar to diesel and therefore can be used in diesel engine without any engine modification, as was confirmed by (Jalaludin *et al.,* 2020; K. Kumar & Sharma, 2016; Sabapathy *et al.,* 2021). The physicochemical properties were evaluated according to ASTM D7467 and EN 14214 and EN 14213 international standards.

3.3.2 Dispersion of GNPs to Oleander-Croton biodiesel/Diesel blend

To prepare 50 ppm sample, the GNPs were weighed accurately at a mass of 50 mg using a precision electronic balance and dispersed in a 2000 ml beaker containing 1 litre of OCB20 and mixed thoroughly using an ultrasonicator (Hielscher ultrasonic Model UP200S40) set at a frequency of 24 kHz, for 40 minutes, to prevent GNPs agglomeration in the OCB20 blend. The sample formed was denoted by GNP50-OCB20. The procedure was repeated for 75 ppm and 100 ppm to prepare GNP75-OCB20 and GNP100-OCB20 samples, respectively. The 50-100 ppm GNPs range was informed by a previous investigation by Debbarma *et al.,* (2020). The stability of the prepared samples was investigated using sedimentation and centrifugation techniques (Saxena, Kumar & Saxena 2017) and was found stable and homogeneous for approximately 96 hours. Thereafter, the viscosity, density and calorific value of the sample fuels were measured using Redwood Viscometer model AN-823 manufactured by Nihon Abura Shikenki, Tokyo-Japan, hydrometer and adiabatic bomb calorimeter manufactured by Yoshida Seisakusho co, ltd Tokyo-Japan, respectively, using D- 445, D-1298 and D-240 ASTM testing methods respectively. The results were compared with those of EN14214, EN 14213 and ASTM 7467 international standards for

conformity. The prepared samples were tested on a stationary single cylinder four-stroke multi-fuel CI engine and performance parameters, including, BSFC and BTE as well as NOx, UHC and CO emissions investigated.

3.4 Engine experimental setup

The experimental set-up consists of a four-stroke, single-cylinder compression ignition engine integrated with an eddy current dynamometer for loading and controlling the speed of the engine. The setup comprises a separate panel box that consists of a fuel tank, air box, fuel gauge unit, and fuel and air gauge transmitters. Measurement of calorimeter water and the engine cooling water flow rates is accomplished with the aid of a rotameter. A proximity switch connected to the engine shaft is used to determine the instantaneous position of the piston TDC while the crank angle is determined using a crank encoder with a resolution of 1°, 5500 RPM with a TDC pulse. Piezoelectric pressure sensor model 601A was employed for measuring instantaneous in-cylinder pressure while the temperature of exhaust gases and cooling water was determined using K-type thermocouples. Signals from the pressure sensor, air flow sensor, speed sensor, load sensor, crank angle sensor and fuel flow sensor are transmitted to the Data Acquisition Device model NI USB6210, 16-bit, 250kS/s and controlled by ICEngineSoft 9.0 software, developed by Apex Innovations Pvt Ltd-India. A Testo Eassy Emission analyzer 350 (software 2.9) and calorimeter are attached to the engine exhaust for the measurement of emissions and estimation of the heat carried away by exhaust gases, respectively. Table 3.2 shows the specifications of the engine while Table 3.3 shows the specifications of the emissions analyzer.

Table 3.2: Specifications of the CI engine

Engine parameters	Specifications
Engine model	Kirloskar, 1 cylinder, 4-stroke, diesel engine
Bore and Stroke	87.5 mm,110 mm
Compression ratio range	12:1–18:1
Stroke	110 mm
Cooling system	Water cooled
Rated power	3.5 kW@1500 rpm
Injection variation	0-25° BTDC
Capacity	661 cc

Table 3.3: Specifications of the exhaust gas analyzer

Gas	Measuring range	Resolution	Accuracy
CO	0 – 5000 ppm	1 ppm	±5% of reading or ±10 ppm
CO_2	0 – 20% by vol.	0.1% by vol.	0.5% of reading
UHC	0–40000 ppm	1 ppm	±0.3% of reading
NOx	0 – 500 ppm	1 ppm	±5% of reading or ±5 ppm
O_2	0 – 25% by vol.	0.01% by vol.	±0.3%

3.5 Performance characteristics

Performance characteristics which included brake power, brake thermal efficiency and brake specific fuel consumption were studied and analysed to aid in determination of the engine torque. The analysis is presented in the following subsections.

3.5.1 Brake power (BP)

It is defined as the power developed by the engine at the output shaft.

$$BP\ (KW) = \frac{2\pi NT}{60 \times 1000} \tag{3.1}$$

Where T is the torque in NM and N is the speed in RPM.

3.5.2 Brake thermal efficiency (BTE)

Brake Thermal Efficiency is the ratio of the power input to the engine in form of fuel power to the power output from the engine shaft. It specifies the ability of the engine to convert chemical energy in the fuel to mechanical power.

$$BTE\ (\%) = \frac{BP}{Fuel\ flow(kg/hr) \times calorific\ value} \tag{3.2}$$

3.5.3 Brake Specific Fuel Consumption (BSFC)

BSFC is the specific amount of fuel consumed against the brake power generated.

$$BSFC\ (kg/kwh) = \frac{Fuel\ flow(kg/hr)}{BP} \tag{3.3}$$

3.6 Engine Test

Engine performance tests were conducted on a stationary single-cylinder four-stroke CI engine with a compression ratio set at 17.5:1 and loads of 0%, 25%, 50%, 75% and 100% chosen based on previous experiments conducted on the same engine. The fuel tank was filled with diesel and ran for approximately 10 minutes to attain steady-state conditions, after which measurements were recorded at zero set load at a constant speed of 1250 rpm.

Measurement of CO, UHC and NOx emissions was accomplished using an emissions analyzer while engine performance characteristics (BTE and BSFC) were obtained using ICEngineSoft 9.0 software. Ten consecutive emission values for every fuel sample were recorded and averaged for accuracy. After taking measurements at no load, the engine was then loaded to 25%, 50%, 75%, and finally to 100% loads, each

load at a time, for every sample after which emissions and engine performance characteristics were recorded.

The neat diesel was then drained and the tank was filled with the OCB20 blend and other samples, each at a time and the process repeated. For every load, the engine parameters were recorded and transmitted to the Data Acquisition Device for analysis and subsequent conversion from analogue to digital format, then displayed in real-time on the DAQ PC, in both graphical & numerical formats. Eventually, the engine was run on neat diesel to flash out any residuals of the sample fuel from the injection system. The schematic of the engine setup is illustrated in Figure 3.1.

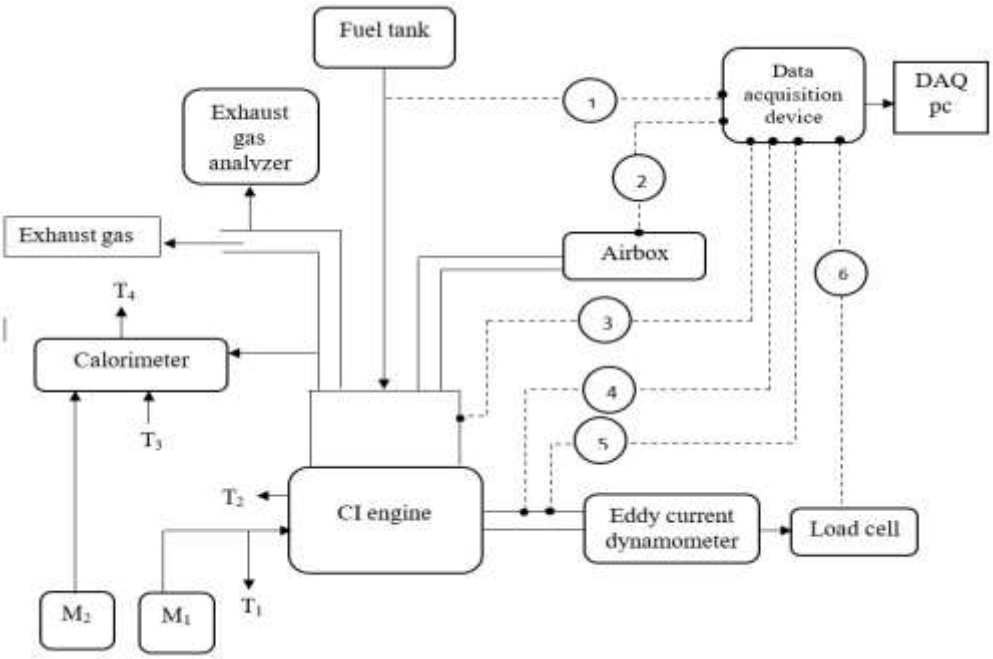

1. Fuel flow sensor **4**. Speed sensor **T_1** Temperature of cooling water to the engine **T_4** Temp. of cooling water from calorimeter

2. Air flow sensor **5**. Crank angle sensor **T_2** Temperature of cooling water from the engine **M_1** Engine cooling water flow meter

3 .Pressure sensor **6.** Load sensor **T_3** Temperature of cooling water to calorimeter **M_2** Calorimeter cooling water flow meter

Figure 3.1: Schematic of the engine setup

3.6 Experimental Uncertainty

Uncertainty analysis is essential for quantifying the uncertainty in the measured data. It aids in determination of the repeatability and precision of the experimental results. The sources of error include instruments used for the measurement, human errors or environmental conditions. The size of the error was minimized by considering the mean of three readings under a constant operating condition, which showed a spread about the mean. The current study employed a student's t-test for the error analysis since the sample size was small. The mean ($\bar{x}$), Variance ($\sigma^{2)}$ and standard deviation (σ) for the sample size (n) were obtained using equations (3.4), (3.5) and (3.6), respectively while the error was calculated using equation (3.7) (Jeyaseelan & Chako, 2020).

$$\bar{x}=\frac{1}{n}\sum_{i=1}^{N} x_i \tag{3.4}$$

$$\sigma^2 = \frac{1}{n-1}\sum_{i=1}^{N}(x_i - \bar{x})^2 \tag{3.5}$$

$$\sigma = \left(\frac{1}{n-1}\sum_{i=1}^{N}(x_i - \bar{x})^2\right)^{\frac{1}{2}} \tag{3.6}$$

$$Error, \Delta = \frac{t \times \sigma}{n} \tag{3.7}$$

Where t is the value obtained from student's t-table with a degree of freedom of n -1 at 95% confidence level (or 0.05 significance level).

The error margin for BTE and BSFC for the 5 fuel samples tested is as shown in Table 3.4 while that of CO, HC and NO_X is ± 5%, ± 0.3% and ± 5% respectively, provided by the manufacturer. From the table, it can be seen that the values for the mean for the three runs in each treatment are less than 0.05 implying there is no significant difference between the values obtained for each run for the treatment in consideration. Table 3.5 shows the measurement range and accuracy of instruments used in the study.

Table 3.4: Error margin for BTE and BSFC at 95% confidence level and degree of freedom of n-1

Test fuels	Parameter measured	
	BTE	BSFC
D100	± 0.024	± 0.0024
OCB20	± 0.051	± 0.0014
GNP50-OCB20	± 0.051	± 0.0024
GNP75-OCB20	± 0.030	± 0.0024
GNP100-OCB20	± 0.033	± 0.0014

Table 3.5: Accuracy of measuring instruments

S/no.	Instrument	Measuring range	Accuracy (±)
1	Dynamometer	560 Nm	1.68 Nm
2	Air flow meter	160 m^3/h	1m^3/h
3	Pressure sensor	0-250 bar	1.118%
4	Thermocouples	0-1300 K	1 $^{\circ}C$
5	Load indicator	250-5000 W	10 W
6	Crank angle encoder, degree	0–720	0.5
7	Speed sensor, rpm	0–10,000	5 rpm
8	Fuel burette, cc	153	0.2
9	Torque indicator, Nm	0–200	±1% of reading

3.7 Research instruments

The research instruments and their functions are listed in Table 3.6.

Table 3.6: List of Research Instruments

S/No.	Instrument	Specifications	Function
1.	Compression ignition engine	1 cylinder, 4 stroke, water cooled, stroke 110 mm, bore 87.5 mm. Capacity 661 cc. Power 3.5 kW, Speed 1500 rpm, CR range 18:1. Injection variation: 0-25° BTDC injection pressure 205 bar.	Conversion of chemical energy stored in the fuel to mechanical energy.
2.	Dynamometer	Eddy current, water cooled, with loading unit.	Measurement and control of the effective torque and engine speed.
3.	Exhaust gas analyser	Testo easy emission software 2.9.	Measurement of CO, UHC, and NOx emissions
4.	Fuel tank	Capacity 15 liters duel compartment, with fuel metering pipe of glass	Storage of diesel and biodiesel
5.	Magnetic stirrer	REMI 1MLH Maximum stirrer volume 5 liters.	OCB20 blending and dispersion of GNPs to OCB20
6.	Data acquisition device	NI USB 6210, 16 bits, 250 kS/s	Data acquisition and storage.
7.	Software	ICEngineSoft Engine 9.0	Engine Performance Analysis
8.	Redwood viscometer,	AN-823 Nihon Abura shikenki	Determination of Kinematic viscosity
9.	Adiabatic bomb calorimeter	Nenken-Type-Yoshida Seikakusho Co. Ltd.	Determination of Calorific value
10.	Kistler piezoelectric pressure transducer	Model 601A, pressure range-0 to 250 bar, sensitivity of 16.5 pc/bar and accuracy of 1.118%.	Recording the instantaneous in-cylinder pressure.
11.	Crank angle sensor	Resolution 1 Deg. Speed 5500 RPM with TDC pulse.	Crank angle detection
12.	Temperature sensor	Type RTD, PT100 and Thermocouple, Type K	Temperature measurement
13.	Proximity switch	Type: LM12-3004NA	Determination of instantaneous position of TDC.
14.	Fuel flow transmitter	DP transmitter, Range 0-500 mm WC	Control of fuel flow rate

S/No.	Instrument	Specifications	Function
15.	Air flow transmitter	Pressure transmitter, Range (-) 250 mm WC	Control of air flow rate
16.	Calorimeter	Type: Pipe in pipe	Estimation of the heat carried away by exhaust gases
17.	Rotameter	Engine cooling 40–400 LPH; calorimeter 25–250 LPH	Engine and calorimeter cooling water flow rate measurement

3.8 Data Processing and Analysis

Data from the data acquisition device was analyzed and displayed in real-time on the DAQ PC, in both graphical & numerical formats using Engine Performance Analysis software package ICEngineSoft 9.0 while emissions were analyzed using Testo Eassy Emission analyser 350 (software 2.9). Results of characterization of test fuels and GNPs were presented graphically using Origin software.

CHAPTER FOUR

RESULTS AND DISCUSSIONS

4.1 Characterization of Biodiesel and Graphene Nanoparticles

The chemical composition of the biodiesel and GNPs was ascertained through Fourier-Transform Infrared (FT-IR) analysis which identified the presence of various functional groups in the biodiesels and graphene nanoparticles. The experiment was conducted using Bruker Alpha FTIR Spectrometer Model Vertex 70, at a wavelength range of 4000-500 cm^{-1}. The surface and morphological characterization of GNPs, on the other hand, was investigated using Scanning Electron Microscope (JEOL JCM 7000).

4.1.1 FTIR Analysis for Biodiesels and Petroleum Diesel

FTIR analysis was conducted on Oleander and Croton biodiesel, Petroleum diesel and OCB20, and the spectrum for the fuels compared, as illustrated in Figure 4.1. The appearance of strong absorption peaks at approximately 1750 cm^{-1} for Oleander biodiesel, Croton biodiesel and OCB20 spectra represents C=O stretching vibrations which indicates the presence of an ester carbonyl bond (Nandiyanto Oktiani, & Ragadhita, 2019), while those at approximately 1165 cm^{-1} represents C-O stretching vibrations. The appearance of these two sets of peaks confirms the presence of an ester group in the biodiesel. These peaks were absent in the diesel fuel because the latter as no oxygen content nor the ester group in its structure (Ruhul, Kalam, Masjuki, Fattah, Reham, & Rashed,2015). The absorbance peaks observed at approximately 2860 cm^{-1} and 2970 cm^{-1} for all the fuel samples revealed the existence of symmetric and antisymmetric stretching vibrations of the C-H bond in CH_3 and CH_2 groups, respectively, while those at approximately 1480 cm^{-1} and 723 cm^{-1} represented Methylene C-H bend, both of which belong to the alkanes family. The existence of C-H bonds (hydrocarbon) is an indicator that the molecules under investigation have the potential to be used as fuels. High transmittance at a frequency implies there are few bonds to absorb that light in the sample, while low transmittance means there more bonds which have vibrational energies corresponding to the incident light, thus fossil

diesel recorded the highest percentage transmittance, which was attributed to the existence of fewer bonds compared to the other fuel samples.

The percentage transmittance for the OCB20 was lower than that of diesel which pointed to the introduction of more bonds in the sample that absorbed the energy at that particular wavenumber. Coronado *et al.,* (2017; Qasim *et al.,* (2017) reported similar FTIR spectra results from waste vegetable oil blended with petroleum diesel at different concentrations, and a mixture of waste Canola and waste transformer oils blended with petroleum diesel, respectively.

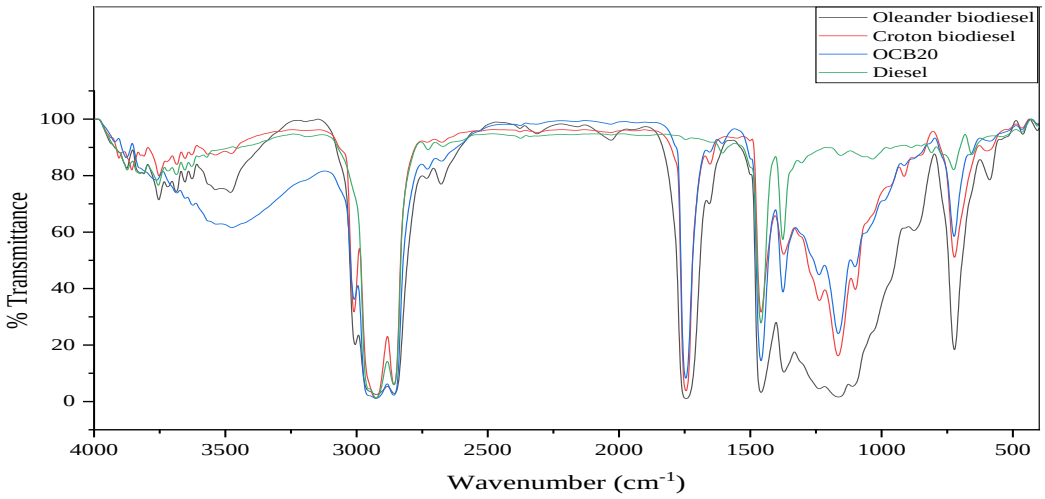

Figure 4.1: FTIR spectrum of Oleander and Croton biodiesel, OCB20 and Petroleum diesel.

4.1.2 FTIR Analysis for GNPs

The chemical structure of GNPs was ascertained using the FTIR spectrum as depicted in Figure 4.2. The absorption peaks at 1070.24 cm^{-1} and 1114.13 cm^{-1} corresponds to large rings of C-O stretching vibrations belonging to the oxy compound functional group (Nandiyanto *et al.,* 2019). The presence of this oxygen-containing bond was attributed to the oxygen residue during graphene exfoliation from graphite oxide (Moosa & Abed, 2021). The sharp narrow peak observed at 1399.86 cm^{-1} was attributed to the C–C stretch (in ring) vibrations in the aromatic ring while the peak at 1597.10 cm^{-1} indicates the presence of C=C-C aromatic ring stretch vibration

(Nandiyanto *et al.,* 2019) which is a dominant covalent bond in the graphene structure (Kamel *et al.,* 2019). The peak at 3131.87 cm^{-1} denoted the existence of an aromatic C-H stretching mode (Nandiyanto *et al.,* 2019). Both 1597.10 cm^{-1} and 3131.87 cm^{-1} peaks belong to the arly functional group to which graphene is a member (Ujjain *et al.,* 2019).

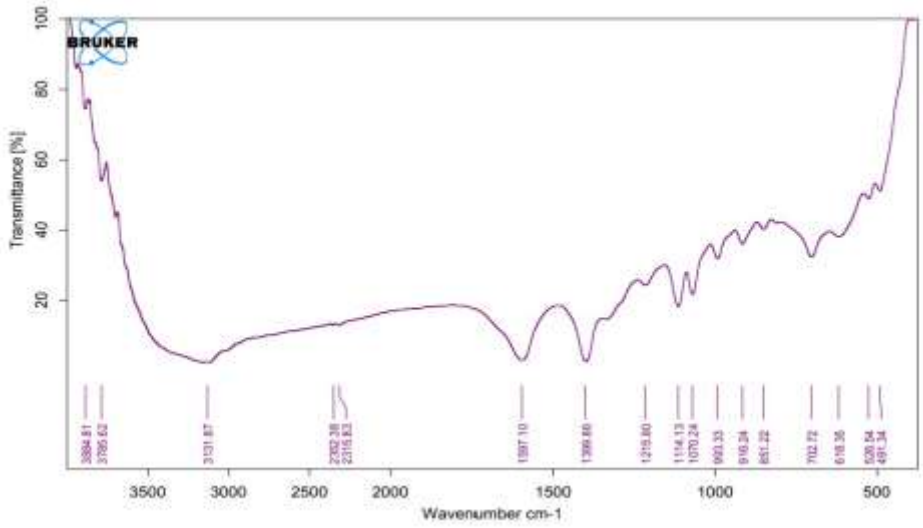

Figure 4.2: Spectrum of GNPs

4.1.3 SEM Analysis for GNPs

The structure, shape and form of the crystals is very important in nanocomposites as it helps to evaluate the mechanical and chemical properties of the nanoparticles under investigation. Figure 4.3 (a) and (b) shows SEM images of GNPs at x500 and x2000 magnification, respectively. The images show that the nanoparticles are spherical, with a flaky surface of approximately 5.0 μm wide, amorphous (Antidormi, Colombo, & Roche, 2022), and are clustered. A closer look at Figure 4.3 (b) reveals the corrugated structure of graphene (Deng & Berry, 2016), which contributes significantly to its high surface area leading to enhanced heat transfer (Begag, Saim, Abboudi & Öztop 2021).

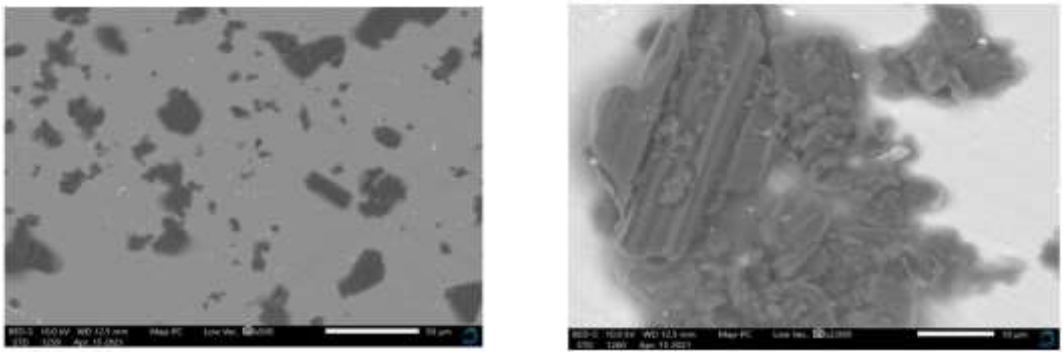

(a) (b)

Figure 4.3: SEM images of GNPs at (a) x500 magnification and (b) x2000 magnification

4.1.4 Comparison of FTIR Spectra for OCB20, Petroleum Diesel and GNPs-Enhanced Fuels.

The FTIR spectra for petroleum diesel, OCB20 and OCB20 enhanced with GNPs at 50 ppm, 75 ppm and 100 ppm concentrations were analyzed and presented as shown in Figure 4.4. The peak at wave number 3500 cm^{-1} was strong and broad for the OCB20 sample compared to that of the petroleum diesel and nano-enhanced samples, with that for petroleum diesel being the weakest. This was attributed to the existence of hydroxyl functional group O-H which is absent in graphene (Kamel *et al.,* 2019) and petroleum diesel (Masera & Hossain, 2017). OCB20 recorded the lowest intensity peaks (percentage transmittance) especially at approximately 1730 cm^{-1}, 1480 cm^{-1}, 1165 cm^{-1} and 725 cm^{-1} compared to those of petroleum diesel and GNP-enhanced samples. The reason could have been that; C=C and C-C bonds in GNPs have a higher peak intensity of approximately 10% compared to the C-O, C=O and C-H bonds in biodiesel which is less than 5%, as can be seen in the GNPs IFTR spectrum (Figure 4.2). The increase in peak intensities in the FTIR spectra points to the inclusion of GNPs in the biodiesel blend.

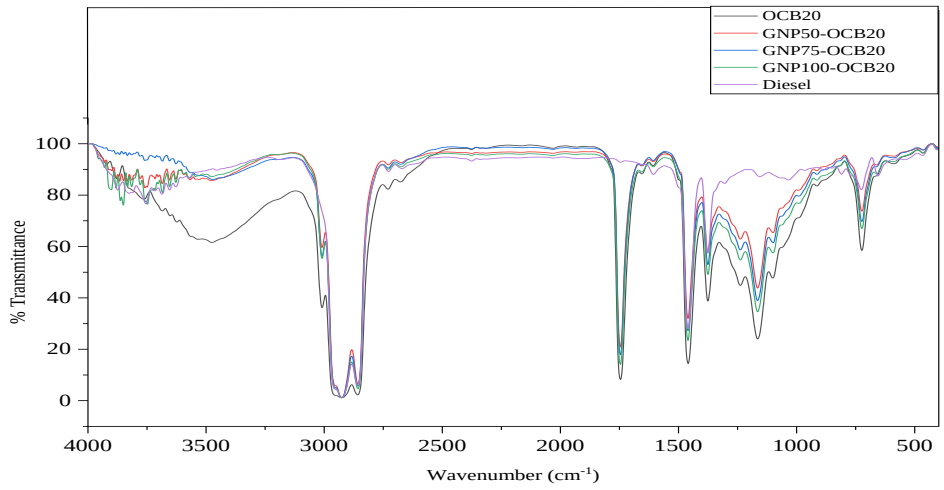

Figure 4.4: FTIR spectra for petroleum diesel, OCB20 and OCB20 enhanced with GNPs at 50 ppm, 75 ppm and 100 ppm

4.2 Fuel Physicochemical Properties

The physicochemical properties of D100, OCB20, GNP50-OCB20, GNP75-OCB20 and GNP100OCB20 fuels were measured according to the prescribed testing methods and the results were compared with those of EN14214 and ASTM 7467 standards for conformity. Table 4.1 presents the physicochemical properties of the test fuels.

Table 4.1: Properties of the test fuels

Fuel Property	Testing method	Diesel	OCB20	GNP50-OCB20	GNP75-OCB20	GNP100-OCB20	EN14214
Density @15 °C, g/cm^3	ASTM D-1298	0.827	0.850	0.852	0.854	0.856	0.860-0.900
Kinematic viscosity @ 40 °C, mm^2/s	ASTM D-445	2.02	3.60	8.638	8.756	9.757	3.5 - 5.0
Calorific Value, MJ/kg	ASTM D-240	42.462	41.759	42.657	41.427	41.167	-

4.2.1 Density

The density of OCB20 was higher than that of petroleum diesel, which was probably due to the large molecular mass and chemical structure of the biodiesel (Mahmudul *et*

al., 2017). GNPs-enhanced biodiesel on the other hand, recorded a density of between 0.852 g/cm^3 and 0.856 g/m^3 which was higher than that of petroleum diesel and OCB20. This was attributed to the inclusion of GNPs (Kannaiyan *et al.,* 2017). A similar trend was observed by Mallikarjuna *et al.,* (2022) who doped a blend of 20% Jatropha methyl ester + 80% diesel (JME20) with graphene nanoparticles (GNPs) at 25 ppm, 50 ppm, 75 ppm and 100 ppm concentration and obtained densities of 0.852 g/m^3, 0.857 g/cm^3, 0.866 g/cm^3 and 0.873 g/cm^3 for JME20, JME20+50GNPs, JME20+75GNPs and JME20+100GNPs fuels, respectively. These results however, deviated slightly from those of EN14214 European standards which range between 0.860-0.900 g/cm^3 (European Committee for Standardization, 2014).

4.2.2 Kinematic Viscosity

Petroleum diesel recorded the lowest kinematic viscosity of 2.02 mm^2/s, while GNP50-OCB20, GNP75 OCB20 and GNP100OCB20 recorded 8.638 mm^2/s, 8.756 mm^2/s and 9.757 mm^2/s, respectively, which was higher than that of OCB20 (3.60 mm^2/s) and that stipulated by ASTM D6751, ASTM D7467 and EN 14214 international standards which is 1.9-6.0 mm^2/s (Sakthivel *et al.,* 2018), 1.9-4.1 mm^2/s (AFDC, 2015) and 3.5-5.0 mm^2/s (European Committee for Standardization, 2014), respectively. This increase was attributed to the presence of GNPs in the OCB20 which increased the friction at the fluid/surface interface due to GNPs/surface collisions and other interlayer resistance and interfacial forces (Kannaiyan *et al.,* 2017). High viscosity reduces fuel atomization which leads to poor combustion resulting in low brake thermal efficiency (Bidir *et al.*, 2022).

4.2.3 Calorific Value

GNP50-OCB20 recorded the highest calorific value which was 42.657 MJ/kg. This was attributed to the higher energy density and superb thermal properties of the nanoparticles (Elsaid *et al.,* 2021). However, it reduced slightly with the increase in GNPs concentration owing to the increase in viscosity which probably overrode the high energy density and thermal properties of the GNPs. On the other hand, neat diesel recorded a higher calorific value compared to OCB20 (41.759 MJ/kg), 75ppm (41.427 MJ/kg) and 100 ppm (41.167 MJ/kg) samples which was probably due to the absence

of oxygen content in the diesel fuel (Pham, 2015). The calorific value for the nano-fuels was within the limits prescribed by EN14213 which is 35 MJ/kg (Mujtaba *et al.,* 2023). A similar trend, especially for the nano fuels was observed by Razzaq *et al.,* (2021) who blended 30% palm oil biodiesel and 70% diesel (B30) with 40, 80 and 120 ppm of GONPs and B30GNPDMC10, from which they obtained 44.703 MJ/kg, 43.824 MJ/kg, 41.2994 MJ/kg, 40.687 MJ/kg, 40.657 MJ/kg and 40.390 MJ/kg for Diesel, B30, B30DMC10, B30GNP40DMC10, B30GNP80DMC10 and B30GNP120DMC10, respectively.

4.3 Engine performance characteristics

Engine performance tests were conducted on a stationary CI engine. BTE and BSFC for all fuel samples were analyzed and discussed in the following sub sections.

4.3.1 Brake Thermal Efficiency (BTE)

Variation of BTE with load for D100, OCB20 and fuel blends with GNPs is depicted in Figure 4.5. The BTE recorded at zero load was low but increased with the load up to 75% and then decreased marginally at 100% load. The BTE observed for OCB20 was 13.6% lower than that of D100 while that for GNP50OCB20 was on average 3.48% lower compared to that of D100 and 11.72% higher than that of OCB20 especially at higher loads. GNP75OCB20 recorded the highest BTE overall, which was 2.76% and 18.93% higher than that of D100 and OCB20, respectively, while OCB20 recorded the lowest. BTE for GNP100OCB20 was 2.09% lower than that of D100 and 13.33% higher than that of OCB20.

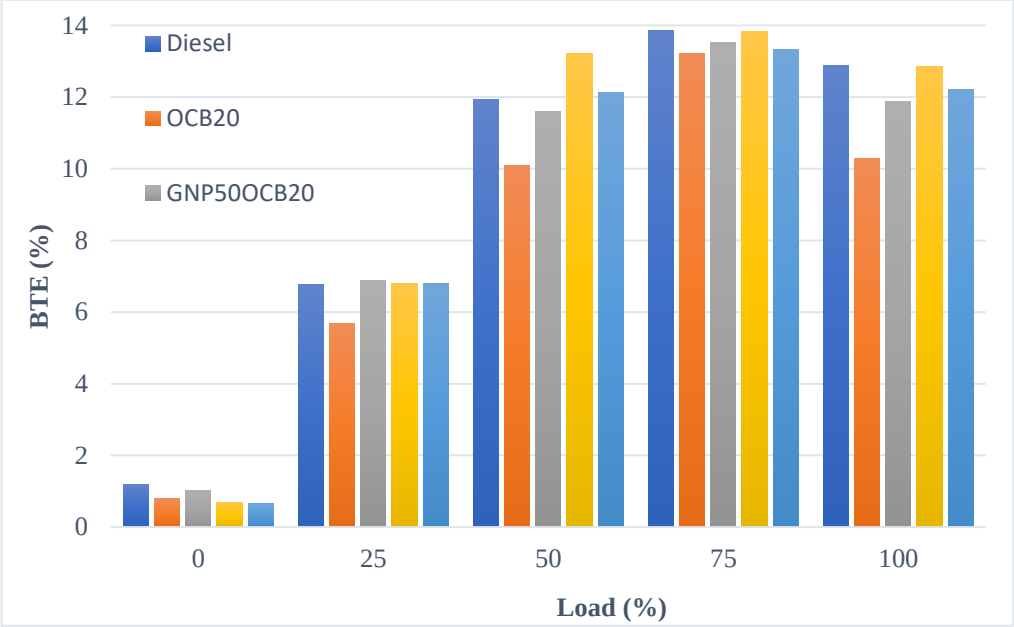

Figure 4.5: Variation of brake thermal efficiency with load

The low BTE at 0% load was attributed to the low fuel supply because the engine was idling. On the other hand, increase in BTE with load was probably due to the increase in the fuel supply, hence availability of more fuel for combustion, while the decrease at full load could have been occasioned by the increased fuel-to-air ratio which reduced the combustion efficiency. This trend agrees with that reported by Debbarma *et al.,* (2020). On the other hand, the reduction in BTE for OCB20 compared to D100 was traced to the reduced CV, increased viscosity and density of the fuel blend relative to D100, while the reduction in relation to the doped fuels was ascribed to the absence of GNPs which resulted in reduced fuel atomization and consequently lowered combustion efficiency. Bhagwat *et al.,* (2015) observed similar results for HOME with GNPs.

The reduction of BTE for the GNP50OCB20 sample relative to D100, more so at higher loads was probably occasioned by the presence biodiesel and GNPs in the fuel blend which increased the density and viscosity of the fuel. On the other hand, its increase compared to OCB20 was possibly due to the increased CV and the inclusion of GNPs which enhanced chemical reactivity and thermal conductivity. Highest BTE recorded for the GNP75OCB20 fuel may have been occasioned by the increase in GNPs concentration which provided a large surface for the chemical reaction to take

place and high catalytic activity which reduced the ignition delay. Besides, the presence of GNPs improved thermal conductivity and oxidation of carbon hence ensuring efficient combustion (El-Seesy, Hassan & Ookawara, 2018). This observation is in line with the findings of Mallikarjuna *et al.,* (2022) for Jatropha biodiesel blend enhanced with GNPs.

The inferior BTE for GNP100OCB20 relative to D100 was attributed to increased concentration of GNPs which increased the density and viscosity of the nanoparticle-enhanced fuel, that not only caused poor fuel atomization during combustion but also may have resulted in degradation of thermal performance of the nano fluid, while the increase relative to OCB20 was probably due to increased catalytic activity and high energy content of GNPs. These results closely agree with those obtained by El-Seesy, Hassan & Ookawara, (2018) and Debbarma *et al.,* (2020) for GNPs in Jatropha biodiesel and GNPs in Palm biodiesel, respectively.

4.3.2 Brake Specific Fuel Consumption (BSFC)

Figure 4.6 illustrates variation of BSFC with engine load for D100, OCB20 and blends with GNPs. From the figure, BSFC is highest at no load condition. It decreases as the load increases up to 75%, then increases marginally at full load. The lowest BSFC was recorded at 75% load for all samples. The BSFC for OCB20 was the highest, which was 17.07% higher than that of D100, while GNP75OCB20 recorded the lowest on average, which was 2.44% and 16.67% lower than that of D100 and OCB20, respectively. GNP100OCB20 on the other hand, recorded a BSFC 1.22% higher than that of D100 and 13.54% lower than that of OCB20.

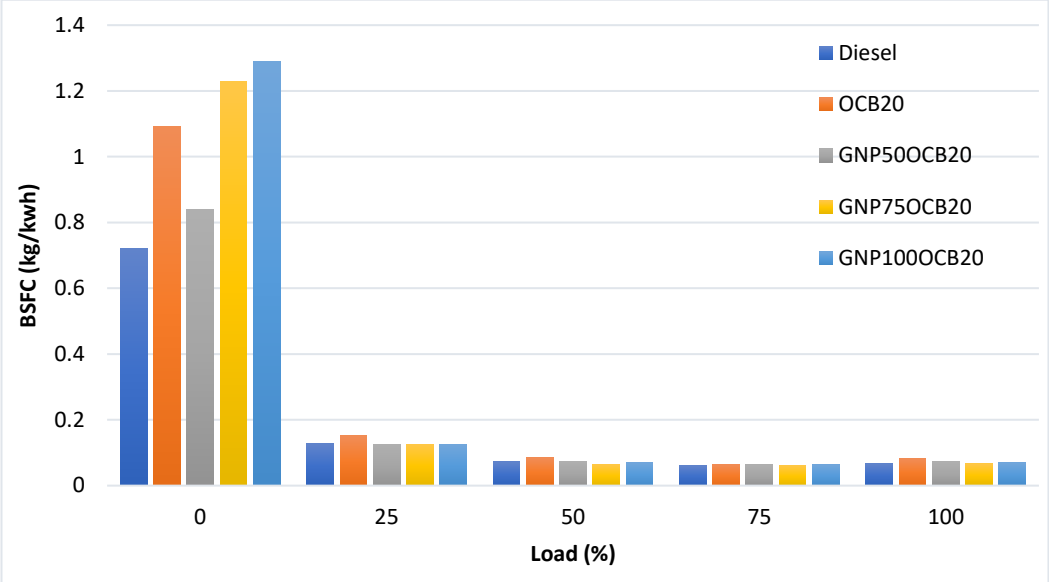

Figure 4.6: Variation of BSFC with load

The BSFC was highest at zero load condition owing to the low temperature in the cylinder which consequently resulted in low fuel conversion efficiency. Nair *et al.,* (2021) noted a similar trend for *Karanja* biodiesel- diesel mixture with GNPs. The reduction in BSFC as the load increased followed by the marginal increment at full load was possibly due to the fact that the engine operates with a lean mixture at lower loads compared to full load conditions. This observation agreed with that of Bidir *et al.,* (2022) for Jatropha (J20) and *Karanja* (K20) biodiesel blends doped with GNPs The high BSFC for OCB20 relative to all other fuels could have been occasioned by the high density, high viscosity and low CV of the blend which resulted in poor fuel atomization and less efficient combustion compared to other fuels, while the reduction in BSFC for GNP75OCB20 was attributed to the increase in the GNPs concentration that resulted in enhanced thermal conductivity and chemical reactivity. The high BSFC recorded for GNP100OCB20 sample compared to D100 was ascribed to the high viscosity, low CV and high density of the fuel compared to D100, while the reduction compared to that of OCB20 could have been as a result of the catalytic effect of the GNPs. These results agreed with those of (Buksagarmath *et al.,* (2018) from a mixture of Simarouba biodiesel with GNPs.

4.4 Emission Characteristics

The effect of GNPs on the CI engine exhaust gas emissions (CO, UHC, NOx) at different engine load conditions was analyzed and the results discussed in the following sections.

4.4.1 Carbon Monoxide (CO)

CO is a toxic hydrocarbon combustion product in CI engine formed as a result of incomplete combustion occasioned by insufficient supply of O_2 molecules. Variation of CO with load for D100, OCB20 and OCB20-GNPs blended fuels is shown in Figure 4.7. CO emission increases slightly at 25% load relative to 0% load but increases significantly at 100% load for all fuel samples. CO emission for OCB20 was the highest, at 16.69% higher than that of D100 while the lowest was achieved with GNP50OCB20, which was 8.58%, 21.65%, 15.87%, and 19.56% lower relative to D100, OCB20, GNP75OCB20 and GNP100OCB20, respectively. On the other hand, CO emission for GNP75OCB20 and GNP100OCB20 samples was higher than that of D100. However, CO emission for GNP75OCB20 was 6.88% lower than that of OCB20.

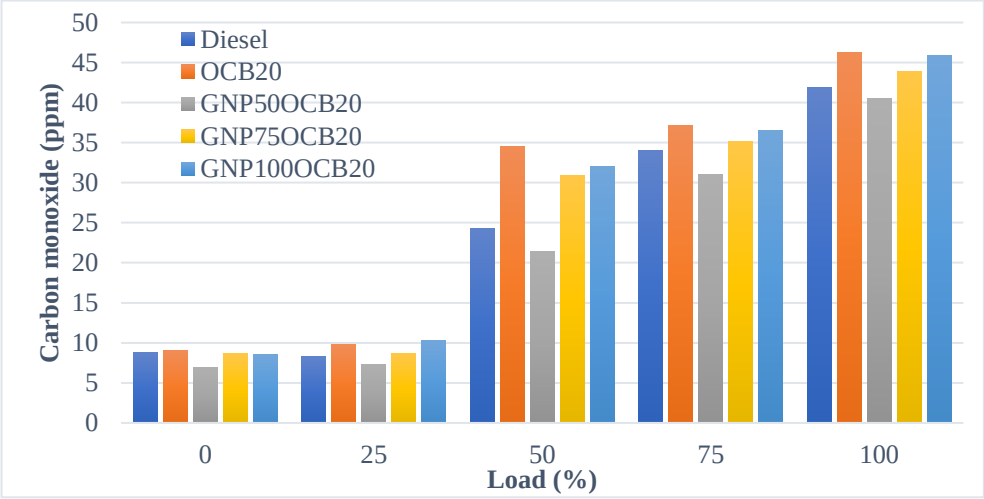

Figure 4.7: Variation of carbon monoxide with load

The marginal increase of CO at no load and low load was attributed to the low fuel supply while the subsequent increase at higher loads was possibly due to the rich fuel mixture hence more emission. The high emissions for OCB20 relative D100 and GNPs-enhanced fuels may have been occasioned by the low CV, high viscosity and high density in relation to D100, and the absence of GNPs, respectively, which resulted in poor air-fuel mixing that led to incomplete combustion. The findings agreed closely with those of Kumar & Sharma, (2016) for WCOME blend with GNPs. The low CO emission achieved for GNP50OCB20 was attributed to improved combustion occasioned by the addition of GNPs to the fuel, which enhanced chemical reactivity and thermal conductivity, and the extra oxygen in the biodiesel, which led to better conversion of CO to CO_2. The high CO emission recorded for GNP75OCB20 and GNP100OCB20 samples compared to D100 may have been as a result of the increased GNPs concentration in the sample fuels which increased viscosity and density of the mixture relative to D100 leading to poor fuel atomization and hence inferior combustion of the fuel. Density and viscosity of the fuel increased with the increase in GNPs dosage, hence higher CO emission for GNP100OCB20 compared to other fuel samples with NPs. These findings are similar to those of Razzaq *et al.,* (2021) for palm biodiesel blends with GONPs and DMCs NPs.

4.4.2 Unburned Hydrocarbon (UHC)

This is a pollutant formed as a result of poor or partial fuel combustion. Variation of UHC emission with load for D100, OCB20 and OCB20-GNPs blended fuels is presented in Figure 4.8. At 0% to 50% loads, HC emission was low but increased for 75% and 100% loads. HC emission for OCB20 was high compared to D100 at 25% and 50% loads, and decreased as the load increased, allowing the UHC emission levels of D100 to be the highest at 75% and 100% loads. The lowest emission level was achieved for the GNPs-enhanced fuels, with GNP50OCB20 recording the lowest which was 52.2% and 50% relative to D100 and OCB20, respectively. However, the UHC emission increased with increase in GNPs dosage, resulting in emissions of GNP75OCB20 and GNP100OCB20 doubling relative to those of GNP50OCB20 samples. A drop of 11.52% and 5.57% for GNP75OCB20 and 7.59% and 1.38% for GNP100OCB20 compared to D100 and OCB20, respectively, was observed.

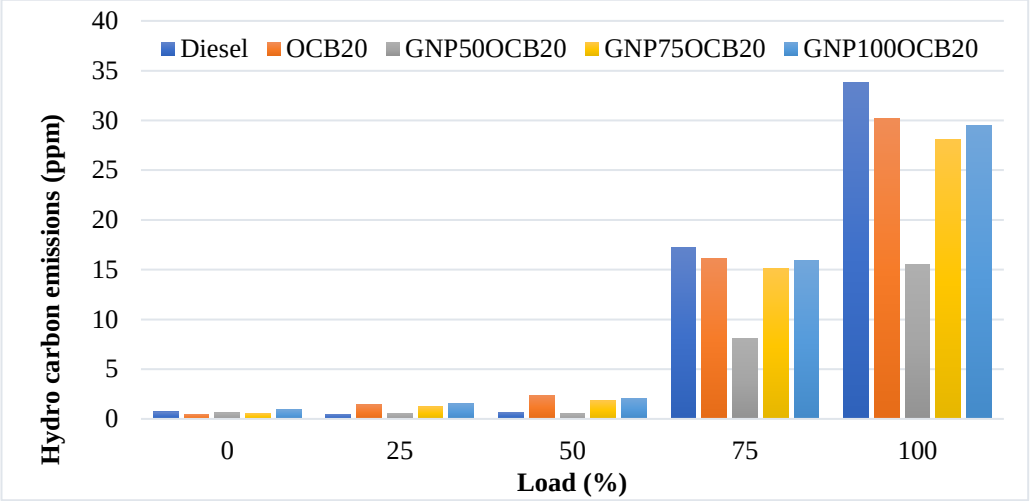

Figure 4.8: Variation of unburned hydrocarbon emission with load

The low UHC emission at low loads and the subsequent increase as the load increased was traced to the fact that at no load and low loads minimal fuel is supplied, hence a lean mixture with improved combustion efficiency. At high loads, the fuel supply is increased to service the load demand, which in turn increases the fuel-air ratio which results in higher UHC emission. This agrees with the findings of Gad *et al.,* (2022). The higher UHC emission for OCB20 compared to D100 at lower loads was probably due to lower CV and high density and viscosity compared to that of D100 which resulted in inferior fuel atomization that led to incomplete combustion. On the other hand, the high UHC for diesel, specifically at higher loads, was attributed to less O_2 available for oxidation of the fuel compared to biodiesel with additional O_2 from its molecular structure (Mahmudul *et al.,* 2017). These findings agreed with those of Debbarma *et al.,* (2020).

GNPs-enhanced fuels recorded the lowest UHC emission with GNP50OCB20 taking the lead. This was ascribed to the high catalytic activity of GNPs coupled with the high O_2 content in the biodiesel which may have improved the combustion of hydrocarbons to products of complete combustion. On the other hand, the increase of emission for GNP75OCB20 and GNP100OCB20 relative to GNP50OCB20 may have been due to the increase in viscosity, density and reduction in CV of GNP75OCB20 and GNP100OCB20 resulting from the higher quantity of GNPs in the fuel blends.

4.4.3 Oxides of Nitrogen (NOx)

NOx is a toxic gas emitted by CI engines as a result of oxygen and nitrogen in the combustion chamber interacting at high temperatures. Its formation is directly proportional to combustion flame temperature inside the cylinder. Variation of NOx with load for D100, OCB20 and GNPs-enhanced fuel samples is demonstrated in Figure 4.9. NOx emission increased alongside load for all samples tested. NOx emitted for nanoparticle-enhanced fuel samples were higher than those of D100 and OCB20, with GNP75OCB20 recording the highest. D100 recorded the lowest.

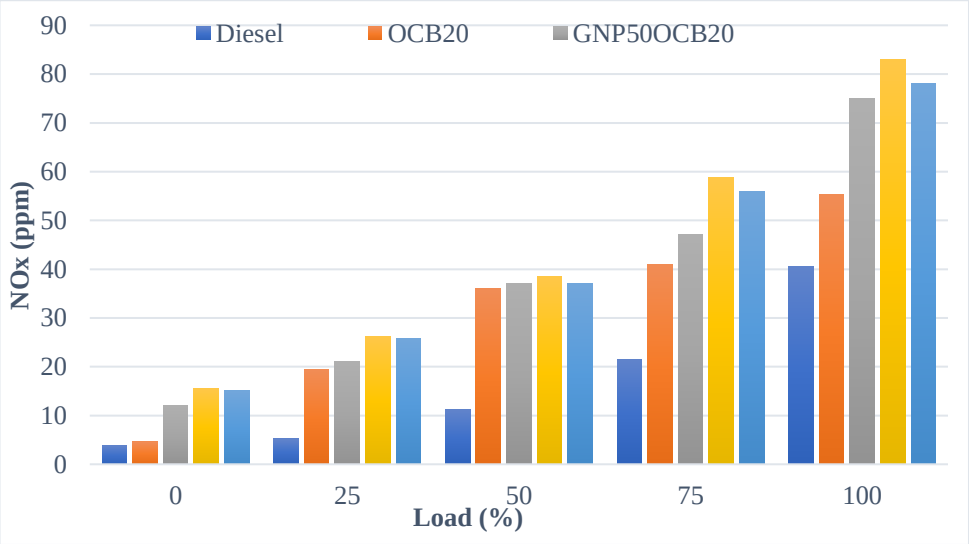

Figure 4.9: Variation of oxides of Nitrogen emission with load

The increase in NOx emission with load for all fuel samples tested was ascribed to the fact that at high load, more fuel is combusted which in turn releases more heat. This results in increased average gas temperature which oxidizes the nitrogen in the air leading to NOx formation. This trend is similar to that observed by Bhagwat *et al.,* (2015). The low NOx emissions recorded for D100 was possibly due to less oxygen to react with nitrogen to form NOx compared to biodiesel, since biodiesel has extra oxygen in its chemical structure (Pham, 2015). Furthermore, the availability of more oxygen facilitated combustion of fuel, which increased the temperature inside the chamber. This high temperature aided the reaction of oxygen with atmospheric nitrogen thereby forming NOx. Mallikarjuna *et al.,* (2022) and Debbarma *et al.,* (2020) reported a similar trend. On the other hand, the high NOx emission for GNPs-enhanced

fuels compared to that of D100 and OCB20 was ascribed to high combustion temperatures resulting from enhanced combustion due to the rich air-fuel mixture occasioned by addition of GNPs. This closely agrees with the findings of Bidir *et al.,* (2022). GNP75OCB20 produced the highest NOx emission possibly due to the high gas temperature in the combustion chamber for that concentration which led to oxidation of some of the nitrogen in the air to NOx, hence the increase in NOx emission.

CHAPTER FIVE

CONCLUSIONS AND RECOMMENDATION

5.1 Conclusions

Performance and emissions characteristics of a compression ignition engine fueled with Oleander/ Croton biodiesel-diesel blend (OCB20) and OCB20 blended with GNPs at mass fractions of 50 ppm, 75 ppm, and 100 ppm were investigated. Doping GNPs to the fuel blend improves brake thermal efficiency by 2.76% and 18.93% and reduces brake specific fuel consumption by 2.44% and 16.67% compared to diesel and OCB20, respectively, at 75 ppm concentration. On the other hand, the presence of GNPs lowers emissions specifically those of carbon monoxide and unburnt hydrocarbon by 8.58% and 21.65%, and 52.2% and 50% respectively, compared to the biodiesel-diesel blend and fossil diesel, respectively, at 50 ppm dosing level. However, it results in an increase in NOx emission in relation to both biodiesel-diesel blend and neat diesel.

It can therefore be concluded that addition of graphene nanoparticles to oleander and croton biodiesel-diesel blend improves engine performance and reduces exhaust emissions compared to the fossil diesel, which was the main objective of the study and research question i. Optimum engine performance was achieved at 75 ppm, while minimum engine emissions were achieved at 50 ppm, which addressed specific objectives 1 and 2 and research question ii. The density of the nano-enhanced fuel was between 0.852 g/cm^3 and 0.856 g/m^3 which compared well to that prescribed by EN14214 standards (0.860-0.900 g/cm^3), while the calorific value was between 41 MJ/kg and 42 MJ/kg which was impressively higher than that set by EN14213 standards (35 MJ/kg). Kinematic viscosity, on the other hand ranged between 8.638 mm^2/s and 9.757 mm^2/s, which was slightly higher than that stipulated by ASTM D6751 and EN14214 international standards which is 1.9 mm^2/s – 6.0 mm^2/s and 3.5 mm^2/s - 5.0 mm^2/s, respectively. This physicochemical properties addressed specific objective 3 and research question iii.

From the conclusions drawn it follows that, Oleander-Croton biodiesel-diesel blend mixed with GNPs can be used as substitute fuel for diesel engines for the improvement of engine performance and reduction of UHC and CO emissions. However, since this is achieved with a slight increase in NOx emission, suitable NOx reduction techniques, such as selective catalytic/ non-catalytic reduction technique can be considered.

5.2 Recommendation

From the present investigation, OCB20 biodiesel enhanced with graphene nanoparticles has proved to be an effective alternative fuel to fossil diesel that can fulfil energy security needs without compromising the engine performance. However, this is achieved with a higher percentage of NOx emission, thus further research may be focused towards reduction of NOx emissions.

REFERENCES

Abbasi, E., Akbarzadeh, A., Kouhi, M., & Milani, M. (2016). Graphene: Synthesis, bio-applications, and properties. *Artificial Cells, Nanomedicine and Biotechnology*, ***44***(1), 150–156. https://doi.org/10.3109/21691401.2014.927880

AFDC. (2015). *Alternative Fuels Data Center: ASTM Biodiesel Specifications*. http://www.afdc.energy.gov/fuels/biodiesel_specifications.html

Agarwal, A. K., Gupta, J. G., & Dhar, A. (2017). Potential and challenges for large-scale application of biodiesel in automotive sector. In *Progress in Energy and Combustion Science* (Vol. **61**, pp. 113–149). https://doi.org/10.1016/j.pecs.2017.03.002

Ahmad, T., Hamid, A., Sharma, A., & Bhardwaj, U. (2017). Thevetia Peruviana: a Multipurpose Medicinal Plant- a Review. *International Journal of Advanced Research*, ***5***(8), 486–493. https://doi.org/10.21474/ijar01/5081

Ahmed, F., Giwa, S. O., Ibrahim, M., & Giwa, A. (2016). Production of biodiesel from Jatropha curcas seed oil using base catalysed transesterification. *International Journal of ChemTech Research*, ***9***(6), 322–332.

Antidormi, A., Colombo, L., & Roche, S. (2022). Emerging properties of non-crystalline phases of graphene and boron nitride based materials. In *Nano Materials Science* (Vol. **4**, Issue 1, pp. 10–17). https://doi.org/10.1016/j.nanoms.2021.03.003

Appavu, P., Madhavan, V. R., Jayaraman, J., & Venu, H. (2019). Palm oil-based biodiesel as a novel alternative feedstock for existing unmodified DI diesel engine. *International Journal of Ambient Energy*. https://doi.org/10.1080/01430750.2019.1636884

Assadian, E., Zarei, M. H., Gilani, A. G., Farshin, M., Degampanah, H., & Pourahmad, J. (2018). Toxicity of Copper Oxide (CuO) Nanoparticles on Human Blood Lymphocytes. In *Biological Trace Element Research* (Vol. **184**, Issue 2, pp. 350–

357). https://doi.org/10.1007/s12011-017-1170-4

Attia, H., Nounou, H., & Shalaby, M. (2018). Zinc oxide nanoparticles induced oxidative DNA damage, inflammation and apoptosis in rat's brain after oral exposure. *Toxics*, ***6***(2). https://doi.org/10.3390/toxics6020029

Basha, J. S., & Anand, R. B. (2014). Performance, emission and combustion characteristics of a diesel engine using Carbon Nanotubes blended Jatropha Methyl Ester Emulsions. *Alexandria Engineering Journal*, *53*(2), 259–273. https://doi.org/10.1016/j.aej.2014.04.001

Basumatary, B., Nath, B., Kalita, P., Das, B., & Basumatary, S. (2020). Yellow Oleander (Thevetia peruviana) Seed as a Potential Bioresource for Industrial Applications. *Mini-Reviews in Organic Chemistry*, ***17***(7), 855–871. https://doi.org/10.2174/1570193X17666191230122142

Basumatary, S. (2014a). Yellow oleander (Thevetia peruviana) seed oil biodiesel as an alternative and renewable fuel for diesel engines: A review. *International Journal of ChemTech Research*, *7*(6), 2823–2840.

Basumatary, S. (2014b). Transesterification of citrus maxima seed oil to biodiesel using heterogeneous catalyst derived from peel and rhizome of Musa balbisiana Colla. *International Journal of ChemTech Research*, *7*(5), 2265–2271.

Begag, A., Saim, R., Abboudi, S., & Öztop, H. F. (2021). Effect of internal and external corrugated surfaces on the characteristics of heat transfer and pressure drop in a concentric tube heat exchanger. In *International Journal of Thermal Sciences* (Vol. **165**). https://doi.org/10.1016/j.ijthermalsci.2021.106930

Bhagwat, V. A., Pawar, C., & Banapurmath, N. R. (2015). Graphene Nanoparticle - Biodiesel Blended Diesel Engine. *International Journal of Engineering Research & Technology (IJERT)*, ***4***(02), 75–78. www.ijert.org

Bhardwaj, D., Shukla, A., Maurya, S., Singh, M., Uttam, K., & Gopal, R. (2017). The impact of metal nanoparticles on our environment. In *Incredible World of*

Biotechnology (pp. 163–175).

Bhattacharyya, S. (2022). Transesterification of Yellow Oleander seed oil, its utilization as biodiesel and performance evaluation. *Heliyon*, ***8***(4), e09250. https://doi.org/10.1016/j.heliyon.2022.e09250

Bidir, M. G., Millerjothi, N. K., Adaramola, M. S., & Hagos, F. Y. (2021). The role of nanoparticles on biofuel production and as an additive in ternary blend fuelled diesel engine: A review. *Energy Reports*, ***7***(November), 3614–3627. https://doi.org/10.1016/j.egyr.2021.05.084

Bidir, M. G., Narayanan Kalamegam, M., Adaramola, M. S., Hagos, F. Y., & Chandra Singh, R. (2022). Investigation of combustion, performance, and emissions of biodiesel blends using graphene nanoparticle as an additive. *International Journal of Engine Research*, *May*. https://doi.org/10.1177/14680874221097574

Bolotin, K. I., Sikes, K. J., Jiang, Z., Klima, M., Fudenberg, G., Hone, J., Kim, P., & Stormer, H. L. (2008). Ultrahigh electron mobility in suspended graphene. *Solid State Communications*, ***146***(9), 351–355. https://doi.org/10.1016/j.ssc.2008.02.024

Bora, M. M., Gogoi, P., Deka, D. C., & Kakati, D. K. (2014). Synthesis and characterization of yellow oleander (Thevetia peruviana) seed oil-based alkyd resin. In *Industrial Crops and Products* (Vol. **52**, pp. 721–728). https://doi.org/10.1016/j.indcrop.2013.11.012

Buksagarmath, P., Banapurmath, N., Rajashekar, C. R., & Khandal, S. (2018). Studies on Effect of Graphene Nanoparticles Addition in Different Levels with Simarouba Biodiesel and Diesel Blends on Performance, Combustion and Emission Characteristics of CI Engine. *Arabian Journal for Science and Engineering*, ***43*.** https://doi.org/10.1007/s13369-018-3121-6

Channappagoudra, M. (2021). Effect of copper oxide nanoadditive on diesel engine performance operated with dairy scum biodiesel. *International Journal of Ambient Energy*, ***42***(5), 530–539. https://doi.org/10.1080/

01430750.2018.1557553

Chehroudi, B. (2016). Applications of Graphene in Fuel Propellant Combustion Chehroudi 26 Applications of Graphene in Fuel/Propellant Combustion. *Graphene Science Handbook*, *May*. www.advtechconsultants.com

Coronado, M. A., Montero, G., García, C., Valdez, B., Ayala, R., & Pérez, A. (2017). Quality assessment of biodiesel blends proposed by the new Mexican policy framework. *Energies*, ***10***(5). https://doi.org/10.3390/en10050631

D'Silva, R., Binu, K. G., & Bhat, T. (2015). Performance and Emission Characteristics of a C.I. Engine Fuelled with Diesel and TiO2 Nanoparticles as Fuel Additive. *Materials Today: Proceedings*, ***2***(4–5), 3728–3735. https://doi.org/10.1016/j.matpr.2015.07.162

Dallatu, Y. A., Agbaji, E. B., & Ajibola, V. O. (2018). The influence of physicochemical characteristics of a non-edible oil of yellow oleander seed on its fuel properties. *Bayero Journal of Pure and Applied Sciences*, ***10***(2), 283. https://doi.org/10.4314/bajopas.v10i2.46

Dandajeh, H. A., Talibi, M., Ladommatos, N., & Hellier, P. (2021). Polycyclic aromatic hydrocarbon and soot emissions in a diesel engine and from a tube reactor. *Journal of King Saud University - Engineering Sciences*, https://doi.org/10.1016/j.jksues.2020.12.007

Daud, S., Hamidi, M. A., & Mamat, R. (2022). A review of fuel additives' effects and predictions on internal combustion engine performance and emissions. In *AIMS Energy* (Vol.**10**, Issue 1). https://doi.org/10.3934/ENERGY.2022001

Debbarma, S., Misra, R. D., & Das, B. (2020). Performance of Graphene added Palm Biodiesel in a Diesel Engine. *Clean Technologies and Environmental Policy*, ***22***(2), 523–534. https://doi.org/10.1007/s10098-019-01800-2

Deng, S., & Berry, V. (2016). Wrinkled , rippled and crumpled graphene : an overview of formation mechanism , electronic properties , and applications. *Biochemical*

Pharmacology, ***19***(4), 197–212. https://doi.org/10.1016/j.mattod.2015.10.002

Deng, Y., Meng, X., Ling, C., Lu, T., Chang, H., Li, L., Yang, Y., Song, G., & Ding, Y. (2022). Nanosized Titanium Dioxide Induced Apoptosis and Abnormal Expression of Blood-Testis Barrier Junction Proteins Through JNK Signaling Pathway in TM4 Cells. *Biological Trace Element Research*, ***200***(12), 5172–5187. https://doi.org/10.1007/s12011-022-03099-5

Devarajan, Y., Munuswamy, D. B., & Mahalingam, A. (2018). Influence of nano-additive on performance and emission characteristics of a diesel engine running on neat neem oil biodiesel. In *Environmental Science and Pollution Research* (Vol. **25**, Issue 26, pp. 26167–26172). https://doi.org/10.1007/s11356-018-2618-6

Doughari, J. H., & Abraham, M. (2021). Antifungal Activity of Jatropha Curcas Linn on Candida Albicans and Candida Tropicalis Associated with Neonatal and Infantile Infections in Yola, Nigeria . *American Journal of Agricultural and Biological Sciences*, ***16***(1), 19–32. https://doi.org/10.3844/ajabssp.2021.19.32

El-seesy, A. I., Attia, A. M. A., & El-batsh, H. M. (2018). *The e ff ect of Aluminum oxide nanoparticles addition with Jojoba methyl ester-diesel fuel blend on a diesel engine performance , combustion and emission characteristics*. ***224***(March), 147–166. https://doi.org/10.1016/j.fuel.2018.03.076

EL-Seesy, A. I., & Hassan, H. (2019). Investigation of the effect of adding graphene oxide, graphene nanoplatelet, and multiwalled carbon nanotube additives with n-butanol-Jatropha methyl ester on a diesel engine performance. In *Renewable Energy* (Vol. **132**). Elsevier B.V. https://doi.org/10.1016/j.renene.2018.08.026

El-Seesy, A. I., Hassan, H., & Ookawara, S. (2018). Effects of graphene nanoplatelet addition to jatropha Biodiesel–Diesel mixture on the performance and emission characteristics of a diesel engine. *Energy*, ***147***, 1129–1152. https://doi.org/10.1016/j.energy.2018.01.108

EL-Seesy, A. I., Hassan, H., & Ookawara, S. (2018). Performance, combustion, and

emission characteristics of a diesel engine fueled with Jatropha methyl ester and graphene oxide additives. *Energy Conversion and Management*, ***166*****,** 674–686. https://doi.org/10.1016/J.ENCONMAN.2018.04.049

Elgharbawy, A. S., Sadik, W. A., Sadek, O. M., & Kasaby, M. A. (2021). A review on biodiesel feedstocks and production technologies. In *Journal of the Chilean Chemical Society* (Vol. **65**, Issue 1, pp. 5098–5109). https://doi.org/10.4067/S0717-97072021000105098

Elsaid, K., Abdelkareem, M. A., Maghrabie, H. M., Sayed, E. T., Wilberforce, T., Baroutaji, A., & Olabi, A. G. (2021). Thermophysical properties of graphene-based nanofluids. *International Journal of Thermofluids*, *10*. https://doi.org/10.1016/j.ijft.2021.100073

European Committee for Standardization. (2014). *EN 14214 Fatty acid methyl esters (FAME) Requirements and test methods*. *June*, 10.

Fayad, M. A., Abed, A. M., Omran, S. H., Jaber, A. A., Radhi, A. A., Dhahad, H. A., Chaichan, M. T., & Yusaf, T. (2022). Influence of Renewable Fuels and Nanoparticles Additives on Engine Performance and Soot Nanoparticles Characteristics. *International Journal of Renewable Energy Development*, ***11***(4), 1068–1077. https://doi.org/10.14710/ijred.2022.45294

Fazal, M. A., Haseeb, A. S. M. A., & Masjuki, H. H. (2013). Investigation of friction and wear characteristics of palm biodiesel. *Energy Conversion and Management*, ***67***, 251–256. https://doi.org/10.1016/j.enconman.2012.12.002

Gad, M. S., Abdel Aziz, M. M., & Kayed, H. (2022). Impact of different nano additives on performance, combustion, emissions and exergetic analysis of a diesel engine using waste cooking oil biodiesel. *Propulsion and Power Research*, ***11***(2), 209–223. https://doi.org/10.1016/j.jppr.2022.04.004

Gadipelli, S., & Guo, Z. X. (2015). Graphene-based materials: Synthesis and gas sorption, storage and separation. *Progress in Materials Science*, ***69***, 1–60. https://doi.org/https://doi.org/10.1016/j.pmatsci.2014.10.004

Goswami, L., Kim, K. H., Deep, A., Das, P., Bhattacharya, S. S., Kumar, S., & Adelodun, A. A. (2017). Engineered nano particles: Nature, behavior, and effect on the environment. In *Journal of Environmental Management* (Vol. **196**, pp. 297–315). https://doi.org/10.1016/j.jenvman.2017.01.011

Hamze, S., Cabaleiro, D., & Estellé, P. (2021). Graphene-based nanofluids: A comprehensive review about rheological behavior and dynamic viscosity. *Journal of Molecular Liquids*, ***325***(March). https://doi.org/10.1016/j.molliq.2020.115207

Hanaki, K., & Portugal-Pereira, J. (2018). *The Effect of Biofuel Production on Greenhouse Gas Emission Reductions* (pp. 53–71). https://doi.org/10.1007/978-4-431-54895-9_6

Hawi, M., Elwardany, A., Ismail, M., & Ahmed, M. (2019). Experimental investigation on performance of a compression ignition engine fueled with waste cooking oil biodiesel–diesel blend enhanced with iron-doped cerium oxide nanoparticles. *Energies*, ***12***(5). https://doi.org/10.3390/en12050798

Hougaard, K. S., Campagnolo, L., Chavatte-Palmer, P., Tarrade, A., Rousseau-Ralliard, D., Valentino, S., Park, M. V. D. Z., de Jong, W. H., Wolterink, G., Piersma, A. H., Ross, B. L., Hutchison, G. R., Hansen, J. S., Vogel, U., Jackson, P., Slama, R., Pietroiusti, A., & Cassee, F. R. (2015). A perspective on the developmental toxicity of inhaled nanoparticles. *Reproductive Toxicology*, ***56***, 118–140. https://doi.org/10.1016/j.reprotox.2015.05.015

Igbokwe, I. O., Igwenagu, E., & Igbokwe, N. A. (2020). Aluminium toxicosis: A review of toxic actions and effects. *Interdisciplinary Toxicology*, ***12***(2), 45–70. https://doi.org/10.2478/intox-2019-0007

Igor Ivanov. (2019). Window To the Future. *Current Digest of the Russian Press, The*, ***71***(048), 17–18. https://doi.org/10.21557/dsp.56774463

Issariyakul, T., & Dalai, A. K. (2014). Biodiesel from vegetable oils. In *Renewable and Sustainable Energy Reviews* (Vol. **31**, pp. 446–471). Elsevier Ltd. https://doi.org/10.1016/j.rser.2013.11.001

Jalaludin, H. A., Abdullah, N. R., Sharudin, H., Asiah, A. R., & Jumali, M. F. (2020). Emission characteristics of biodiesel ratios of 10%, 20%, and, 30% in a single-cylinder diesel engine. *IOP Conference Series: Materials Science and Engineering*, ***834***(1). https://doi.org/10.1088/1757-899X/834/1/012066

Jeyaseelan, T., & Chako, N. (2020). Comparative evaluation of graphene oxide and graphene nanoplatelets as fuel additives on the combustion and emission characteristics of a diesel engine fuelled with diesel and biodiesel blend. *Fuel Processing Technology*, ***204***(January), 106406. https://doi.org/10.1016/j.fuproc.2020.106406

Jonas, M., Ketlogetswe, C., & Gandure, J. (2020). Variation of Jatropha curcas seed oil content and fatty acid composition with fruit maturity stage. *Heliyon*, ***6***(1), e03285. https://doi.org/10.1016/j.heliyon.2020.e03285

Kamel, S., El-Sakhawy, M., Anis, B., & Tohamy, H. A. S. (2019). Graphene's Structure, Synthesis and Characterization; A brief review. *Egyptian Journal of Chemistry*, ***62***(Part 2), 593–608. https://doi.org/10.21608/ejchem.2019.15173.1919

Kannaiyan, K., Anoop, K., & Sadr, R. (2017). Effect of nanoparticles on the fuel properties and spray performance of aviation turbine fuel. *Journal of Energy Resources Technology, Transactions of the ASME*, ***139***(3). https://doi.org/10.1115/1.4034858

Keera, S. T., El Sabagh, S. M., & Taman, A. R. (2018). Castor oil biodiesel production and optimization. *Egyptian Journal of Petroleum*, ***27***(4), 979–984. https://doi.org/10.1016/j.ejpe.2018.02.007

Kumar, K., & Sharma, M. P. (2016). Performance and emission characteristics of a diesel engine fuelled with biodiesel blends. *International Journal of Renewable Energy Research*, *6*(2), 658–662. https://doi.org/10.20508/ijrer.v6i2.3827.g6831

Le Ba, T., Mahian, O., Wongwises, S., & Szilágyi, I. M. (2020). Review on the recent progress in the preparation and stability of graphene-based nanofluids. *Journal of*

Thermal Analysis and Calorimetry, ***142***(3), 1145–1172. https://doi.org/10.1007/s10973-020-09365-9

Lee, W.-Y., & Park, H.-J. (2022). Toxicity of cerium oxide nanoparticles on neonatal testicular development in mouse organ culture. *Reproductive Toxicology*, *111*, 120–128. https://doi.org/https://doi.org/10.1016/j.reprotox.2022.05.014

Madiwale, S., Karthikeyan, A., & Bhojwani, V. (2017). A Comprehensive Review of Effect of Biodiesel Additives on Properties, Performance, and Emission. *IOP Conference Series: Materials Science and Engineering*, ***197***(1). https://doi.org/10.1088/1757-899X/197/1/012015

Mahdi, J. M., & Nsofor, E. C. (2017). Melting enhancement in triplex-tube latent heat energy storage system using nanoparticles-metal foam combination. In *Applied Energy* (Vol. **191**, pp. 22–34). https://doi.org/10.1016/j.apenergy.2016.11.036

Mahmudul, H. M., Hagos, F. Y., Mamat, R., Adam, A. A., Ishak, W. F. W., & Alenezi, R. (2017). Production, characterization and performance of biodiesel as an alternative fuel in diesel engines – A review. In *Renewable and Sustainable Energy Reviews* (Vol. **72**, pp. 497–509). https://doi.org/10.1016/j.rser.2017.01.001

Mallikarjuna Rao, D., Janga, V. S. R., Dhana Raju, V., & Arifa, S. (2022). Impact of Graphene Nanoparticles Addition to Jatropha Biodiesel Blend on the Performance and Emission Characteristics of a Diesel Engine. *Lecture Notes in Mechanical Engineering*, *October*, 825–833. https://doi.org/10.1007/978-981-16-4222-7_90

Manavendra, G., & Banapurmath, N. R. (2017). Performance and Emission Characteristics of Graphene Nano Particle-Biodiesel Blends Fuelled Diesel Engine. *International Research Journal of Engineering and Technology*, ***4***(10). www.irjet.net

Maroyi, A. (2017). Croton megalocarpus Hutch. in Tropical Africa: Phytochemistry, Pharmacology and Medicinal Potential. *Research Journal of Medicinal Plants*,

11(4), 124–133. https://doi.org/10.3923/rjmp.2017.124.133

Masera, K., & Hossain, A. K. (2017). Production, Characterisation and Assessment of Biomixture Fuels for Compression Ignition Engine Application. *International Journal of Mechanical and Mechatronics Engineering*, ***11***(12), 1857–1863.

Masood, M. T., Papadopoulou, E. L., Heredia-Guerrero, J. A., Bayer, I. S., Athanassiou, A., & Ceseracciu, L. (2017). Graphene and polytetrafluoroethylene synergistically improve the tribological properties and adhesion of nylon 66 coatings. *Carbon*, ***123***, 26–33. https://doi.org/https://doi.org/10.1016/j.carbon.2017.07.026

Mbayachi, V. B., Ndayiragije, E., Sammani, T., Taj, S., Mbuta, E. R., & khan, A. ullah. (2021). Graphene synthesis, characterization and its applications: A review. *Results in Chemistry*, ***3***(August), 100163. https://doi.org/10.1016/j.rechem.2021.100163

Mehrali, M., Sadeghinezhad, E., Latibari, S. T., Kazi, S. N., Mehrali, M., Zubir, M. N. B. M., & Metselaar, H. S. C. (2014). Investigation of thermal conductivity and rheological properties of nanofluids containing graphene nanoplatelets. *Nanoscale Research Letters*, ***9***(1), 1–12. https://doi.org/10.1186/1556-276X-9-15

MOOSA, A. A., & ABED, M. S. (2021). Graphene preparation and graphite exfoliation. *Turkish Journal of Chemistry*, ***45***(3), 493–519. https://doi.org/10.3906/kim-2101-19

Mujeeb, M. A., Vedamurthy, A. B., & T, S. C. (2016). Current strategies and prospects of biodiesel production: A review. *Pelagia Research Library Advances in Applied Science Research*, ***7***(1), 120–133. www.pelagiaresearchlibrary.com

Mujtaba, M. A., Kalam, A., Masjuki, H. H., Gul, M., Ahmed, W., Soudagar, M. E. M., & Razzaq, L. (2023). Chapter 2 - Comparative investigation of the suitability of fuel properties of oxygenated biofuels in internal combustion engines. In N. Kumar, K. Mathiyazhagan, V. R. Sreedharan, & M. A. B. T.-A. in O. F. for S. D. Kalam (Eds.), *Advancement in Oxygenated Fuels for Sustainable Development*

(pp. 7–25). Elsevier. https://doi.org/https://doi.org/10.1016/B978-0-323-90875-7.00010-1

Mujtaba, M. A., Masjuki, H. H., Kalam, M. A., Noor, F., Farooq, M., Ong, H. C., Gul, M., Soudagar, M. E. M., Bashir, S., Fattah, I. M. R., & Razzaq, L. (2020). Effect of additivized biodiesel blends on diesel engine performance, emission, tribological characteristics, and lubricant tribology. *Energies*, ***13***(13), 1–16. https://doi.org/10.3390/en13133375

Mukherjee, S., & Paria, S. (2013). Preparation and Stability of Nanofluids-A Review. *IOSR Journal of Mechanical and Civil Engineering (IOSR-JMCE)*, ***9***, 63–69. https://doi.org/10.9790/1684-0926369

Muskens, R. (2014). The Global Jatropha Curcas Hype: What can we learn from the boom and bust of a miracle crop? *Sustainability*, *special*(June), 16.

Nair, J., Prasad Kumar, P., Thakur, A. K., Samhita, & Aravinda. (2021). Influence on emissions and performance of CI engine with graphene nanoparticles blended with Karanja biodiesel. *AIP Conference Proceedings*, ***2317***(February). https://doi.org/10.1063/5.0036142

Nandiyanto, A. B. D., Oktiani, R., & Ragadhita, R. (2019). How to read and interpret ftir spectroscope of organic material. *Indonesian Journal of Science and Technology*, ***4***(1), 97–118. https://doi.org/10.17509/ijost.v4i1.15806

Nanthagopal, K., Ashok, B., Tamilarasu, A., Johny, A., & Mohan, A. (2017). Influence on the effect of zinc oxide and titanium dioxide nanoparticles as an additive with Calophyllum inophyllum methyl ester in a CI engine. *Energy Conversion and Management*, ***146***, 8–19. https://doi.org/10.1016/j.enconman.2017.05.021

Nayak, S. K., Mishra, P. C., Kumar, A., Behera, G. R., & Nayak, B. (2017). Experimental investigation on property analysis of Karanja oil methyl ester for vehicular usage. *Energy Sources, Part A: Recovery, Utilization and Environmental Effects*, ***39***(3), 306–312. https://doi.org/10.1080/15567036.2016.1173131

Ombaka, J., Gachuiri, C., & Abong, G. (2019). *Utiliation of croron seed as a possible animal feed : A review*. ***9***, 178–186.

Osawa, W. O., Onyari, J. M., Sahoo, P. K., & Mulaa, F. J. (2014). Process optimization for production of biodiesel from croton oil using two-stage process. *IOSR Journal of Environmental Science, Toxicology and Food Technology*, ***8***(11), 49–54. https://doi.org/10.9790/2402-081134954

Oseni, M., & Obetta, S. (2012). Evaluation of fatty acids profile of ethyl esters of yellow oleander and groundnut oils as biodiesel feedstock. *American Journal of Scientific and Industrial Research*, ***3***(2), 62–68. https://doi.org/10.5251/ajsir.2012.3.2.62.68

Osorio-González, C. S., Gómez-Falcon, N., Sandoval-Salas, F., Saini, R., Brar, S. K., & Ramírez, A. A. (2020). Production of biodiesel from castor oil: A review. *Energies*, ***13***(10), 1–22. https://doi.org/10.3390/en13102467

Pattanaik, B. P., Jena, J., & Misra, R. D. (2017). The effect of oxygen content in soapnut biodiesel-diesel blends on performance of a diesel engine. *International Journal of Automotive and Mechanical Engineering*, ***14***(3), 4574–4588. https://doi.org/10.15282/ijame.14.3.2017.14.0361

Pham, P. X. (2015). *Influences of Molecular Profiles of Biodiesels on Atomization, Combustion and Emission Characteristics Characterisation of Electrostatically Charged Sprays of Biodiesels View project Turbulent Multi-phase Flows View project*. *March*. https://doi.org/10.13140/2.1.4430.1609

Prakash, V., Peralta-Videa, J., Tripathi, D. K., Ma, X., & Sharma, S. (2021). Recent insights into the impact, fate and transport of cerium oxide nanoparticles in the plant-soil continuum. *Ecotoxicology and Environmental Safety*, ***221***, 112403. https://doi.org/10.1016/j.ecoenv.2021.112403

Praveena, V., Venkatesan, S., & Gupta, T. (2018). Effects of nano additives with biodiesel fuels in internal combustion engines - A Review. *IOP Conference Series: Materials Science and Engineering*, ***402***(1). https://doi.org/10.1088/1757-

899X/402/1/012208

Qasim, M., Ansari, T. M., & Hussain, M. (2017). Combustion, performance, and emission evaluation of a diesel engine with biodiesel like fuel blends derived from a mixture of Pakistani waste canola and waste transformer oils. *Energies*, ***10***(7). https://doi.org/10.3390/en10071023

Razzaq, L., Mujtaba, M. A., Soudagar, M. E. M., Ahmed, W., Fayaz, H., Bashir, S., Fattah, I. M. R., Ong, H. C., Shahapurkar, K., Afzal, A., Wageh, S., Al-Ghamdi, A., Ali, M. S., & EL-Seesy, A. I. (2021). Engine performance and emission characteristics of palm biodiesel blends with graphene oxide nanoplatelets and dimethyl carbonate additives. *Journal of Environmental Management*, ***282***(October 2020), 111917. https://doi.org/10.1016/j.jenvman.2020.111917

Rojas-Sandoval, J. (2022). Cascabela thevetia (yellow oleander). In *CABI Compendium: Vol. CABI Compe*. https://doi.org/10.1079/cabicompendium.53608

Román-Figueroa, C., Cea, M., Paneque, M., & González, M. E. (2020). Oil Content and Fatty Acid Composition in Castor Bean Naturalized Accessions under Mediterranean Conditions in Chile. *Agronomy*, ***10***(8), 1145. https://doi.org/10.3390/agronomy10081145

Ruhul, A. M., Kalam, M. A., Masjuki, H. H., Fattah, I. M. R., Reham, S. S., & Rashed, M. M. (2015). State of the art of biodiesel production processes: A review of the heterogeneous catalyst. *RSC Advances*, ***5***(122), 101023–101044. https://doi.org/10.1039/c5ra09862a

Rupasianghe, C. P., & Gunathilaka, K. S. S. (2018). Disaster Risk Reduction through biodiesel from yellow oleander (Thevetia peruviana). *Procedia Engineering*, ***212***(2017), 591–597. https://doi.org/10.1016/j.proeng.2018.01.076

Sabapathy, S. P., Ammasi, A. M., Khalife, E., Kaveh, M., Szymanek, M., Reghu, G. K., & Sabapathy, P. (2021). Comprehensive assessment from optimum biodiesel yield to combustion characteristics of light duty diesel engine fueled with palm

kernel oil biodiesel and fuel additives. *Materials*, ***14***(15). https://doi.org/10.3390/ma14154274

Sakthivel, R., Ramesh, K., Purnachandran, R., & Mohamed Shameer, P. (2018). A review on the properties, performance and emission aspects of the third generation biodiesels. *Renewable and Sustainable Energy Reviews*, ***82***(November), 2970–2992. https://doi.org/10.1016/j.rser.2017.10.037

Sandhya, M., Ramasamy, D., Sudhakar, K., Kadirgama, K., & Harun, W. S. W. (2021). Ultrasonication an intensifying tool for preparation of stable nanofluids and study the time influence on distinct properties of graphene nanofluids – A systematic overview. In *Ultrasonics Sonochemistry* (Vol. **73**). https://doi.org/10.1016/j.ultsonch.2021.105479

Sang, M., Shin, J., Kim, K., & Yu, K. J. (2019). Electronic and thermal properties of graphene and recent advances in graphene based electronics applications. In *Nanomaterials* (Vol. **9**, Issue 3). https://doi.org/10.3390/nano9030374

Saxena, V., Kumar, N., & Saxena, V. K. (2017). A comprehensive review on combustion and stability aspects of metal nanoparticles and its additive effect on diesel and biodiesel fuelled C.I. engine. *Renewable and Sustainable Energy Reviews*, ***70***, 563–588. https://doi.org/10.1016/j.rser.2016.11.067

Secorun, L. (2017). "This is our future" – Kenya's croton tree touted as new biofuels crop. In *The Guardian* (Issue 1, p. 2000).

Silitonga, A. S., Ong, H. C., Mahlia, T. M. I., Masjuki, H. H., & Chong, W. T. (2014). Biodiesel conversion from high FFA crude jatropha curcas, calophyllum inophyllum and ceiba pentandra oil. *Energy Procedia*, ***61***, 480–483. https://doi.org/10.1016/j.egypro.2014.11.1153

SiSim, H. S., Yetter, R. A., Connell, T. L., Dabbs, D. M., & Aksay, I. A. (2020). (2020). Multifunctional Graphene-Based Additives for Enhanced Combustion of Cracked Hydrocarbon Fuels under Supercritical Conditions. *Combustion Science and Technology*, ***192***(7), 1420–1435. https://doi.org/10.1080/

00102202.2020.1737033

Song, Y., Yu, J., Yu, L., Alam, F. E., Dai, W., Li, C., & Jiang, N. (2015). Enhancing the thermal, electrical, and mechanical properties of silicone rubber by addition of graphene nanoplatelets. *Materials & Design*, ***88***, 950–957. https://doi.org/https://doi.org/10.1016/j.matdes.2015.09.064

Soudagar, M. E. M., Banapurmath, N. R., Afzal, A., Hossain, N., Abbas, M. M., Haniffa, M. A. C. M., Naik, B., Ahmed, W., Nizamuddin, S., & Mubarak, N. M. (2020). Study of diesel engine characteristics by adding nanosized zinc oxide and diethyl ether additives in Mahua biodiesel–diesel fuel blend. *Scientific Reports*, ***10***(1), 1–17. https://doi.org/10.1038/s41598-020-72150-z

Soudagar, M. E. M., Nik-Ghazali, N.-N., Abul Kalam, M., Badruddin, I. A., Banapurmath, N. R., & Akram, N. (2018). The effect of nano-additives in diesel-biodiesel fuel blends: A comprehensive review on stability, engine performance and emission characteristics. *Energy Conversion and Management*, ***178***, 146–177. https://doi.org/https://doi.org/10.1016/j.enconman.2018.10.019

State of Global Air, S. (2020). *Soga-2020-Report-10-26* (pp. 1–28).

Tiwari, S. K., Sahoo, S., Wang, N., & Huczko, A. (2020). Graphene research and their outputs: Status and prospect. *Journal of Science: Advanced Materials and Devices*, ***5***(1), 10–29. https://doi.org/10.1016/j.jsamd.2020.01.006

Tony Pallone. (2018). 13 Reasons Graphene Is a “Wonder Material.” In *Https://Www.Globalspec.Com*. https://www.globalspec.com

Ubulom, P. M. E., Yaro, C. A., & Udoh, U.-A. P. (2021). Repellency and insecticidal properties of seed oil of Jatropha curcas L. against American cockroach, Periplaneta americana L. *The Journal of Basic and Applied Zoology*, ***82***(1). https://doi.org/10.1186/s41936-021-00208-z

Ujjain, S. K., Bhatia, R., & Ahuja, P. (2019). Aziridine-functionalized graphene: Effect of aromaticity for aryl functional groups on enhanced power conversion

efficiency of organic photovoltaic cells. In *Journal of Saudi Chemical Society* (Vol. 23, Issue **6**, pp. 655–665). https://doi.org/10.1016/j.jscs.2018.11.006

United Nations Convention for Climate Change. (2023). *Introduction to land use*. United Nations Commission for Climate Change. https://unfccc.int/topics/introduction-to-land-use

USEPA. (2016). Basic Information about Carbon Monoxide (CO) Outdoor Air Pollution. In *U.S. Environmental Protection Agency*.

Vaknin, Y., Yermiyahu, U., Bar-Tal, A., & Samocha, Y. (2018). Global maximization of Jatropha oil production under semi-arid conditions by balancing vegetative growth with reproductive capacity. In *GCB Bioenergy* (Vol. **10**, Issue 6, pp. 382–392). https://doi.org/10.1111/gcbb.12497

Venkatesan, H., Sivamani, S., Sampath, S., Gopi, V., & Dinesh Kumar, M. (2017). A comprehensive review on the effect of nano metallic additives on fuel properties, engine performance and emission characteristics. *International Journal of Renewable Energy Research*, ***7***(2), 825–843. https://doi.org/10.20508/ijrer.v7i2.5678.g7064

WHO. (2018). Ambient (outdoor) air pollution. In *Https://Www.Who.Int/En/News-Room/Fact-Sheets/Detail/Ambient-(Outdoor)-Air-Quality-and-Health* (Issue 1, pp. 6–8).

Yang, Y., Liu, R., Wu, J., Jiang, X., Cao, P., Hu, X., Pan, T., Qiu, C., Yang, J., Song, Y., Wu, D., & Su, Y. (2015). Bottom-up Fabrication of Graphene on Silicon/Silica Substrate via a Facile Soft-hard Template Approach. *Scientific Reports*, ***5***(July), 1–7. https://doi.org/10.1038/srep13480

Yarkasuwa, C. I., Wilson, D., & Michael, E. (2013). Production of biodiesel from yellow oleander (thevetia peruvian) oil and its biodegradability. *Journal of the Korean Chemical Society*, ***57***(3), 377–381. https://doi.org/10.5012/jkcs.2013.57.3.377

Yusof, S. N. A., Sidik, N. A. C., Asako, Y., Japar, W. M. A. A., Mohamed, S. B., & Muhammad, N. M. az. (2021). A comprehensive review of the influences of nanoparticles as a fuel additive in an internal combustion engine (ICE). In *Nanotechnology Reviews* (Vol. **9**, Issue 1, pp. 1326–1349). https://doi.org/10.1515/ntrev-2020-0104

Zhai, W., Srikanth, N., Kong, L. B., & Zhou, K. (2017). Carbon nanomaterials in tribology. *Carbon*, ***119***, 150–171. https://doi.org/https://doi.org/10.1016/j.carbon.2017.04.027

APPENDICES

Appendix I: Apparatus for measuring fuel physicochemical properties, emissions and data acquisition

Bomb calorimeter

Redwood viscometer

Emissions analyzer

Data Acquisition Device

Appendix II: Physicochemical properties of oleander-croton biodiesel at different ratios

Fuel Property	Testing Method	Croton biodiesel -100%	Oleander biodiesel -100%	Croton-70% Oleander -30%	Croton-60% Oleander -40%	Croton-50% Oleander -50%	Oleander -70 % Croton-30%	Oleander -60 % Croton-40%
Density @15^{o}C, g/cm^{3}	ASTM D-1298	0.940	0.904	0.938	0.930	0.922	0.910	0.915
Kinematic viscosity @40°C, mm^{2}/s	ASTM D-445	24.04	22.35	23.72	23.56	23.45	22.81	23.05
Calorific value, KJ/kg	ASTM D-240	36,312	35,960	36,296	36,281	36,200	36,150	36,050

Appendix III : Equipment used for SEM and FT-IR analyses

Scanning Electron Microscope

Brüker Alpha FTIR Spectrometer

Appendix IV: Preparation of GNPs-enhanced fuels

Blending of Oleander/Croton biodiesel

Graphene nanoparticles

Doping of OCB20 with GNPs

OCB20-GNPs blends

Appendix V: Preparations for data collection at JKUAT thermodynamics laboratory

Confirming rotameter water level

Starting the engine

Loading the engine

Emission data collection

Appendix VI: Data for performance characteristics of the fuel samples

Fossil diesel

Indicated & Brake Thermal Efficiency and SFC & Fuel Consumption

Speed (rpm)	Load (kg)	IThEff (%)	BThEff (%)	SFC (kg/kWh)	Fuel (kg/h)
1261.00	0.46	8.30	1.19	0.72	0.80
1260.00	3.28	25.63	6.76	0.13	1.00
1261.00	6.08	27.13	11.94	0.072	1.05
1240.00	8.54	30.22	13.86	0.062	1.25
1175.00	12.06	20.50	12.88	0.067	1.79

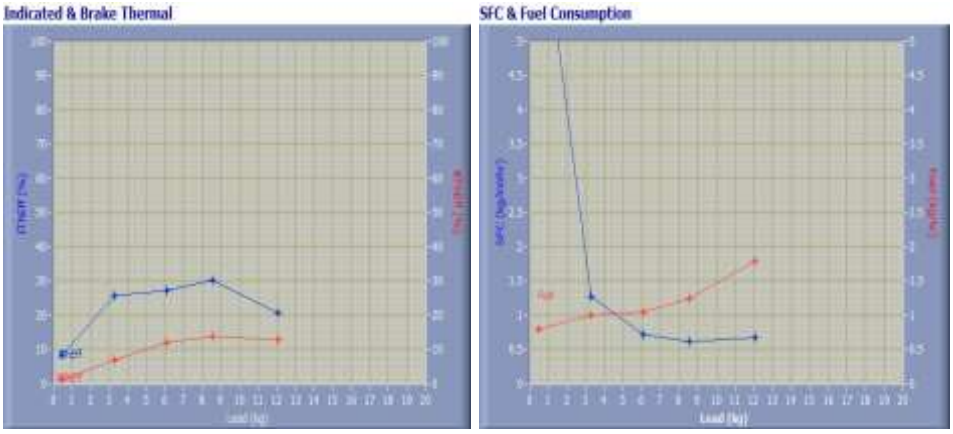

Air & Fuel Flow and Torque, Mechanical & Volumetric Efficiency

Speed (rpm)	Load (kg)	Air (mmWC)	Fuel (cc/min)	Torque (Nm)	Mech Eff. (%)	Vol Eff. (%)
1261.00	0.46	266.78	16.00	0.84	14.29	181.08
1260.00	3.28	266.80	20.00	5.95	26.38	181.23
1261.00	6.08	266.77	21.00	11.03	44.02	181.08
1240.00	8.54	266.80	25.00	15.50	45.85	184.16
1175.00	12.06	266.80	36.00	21.89	62.84	194.34

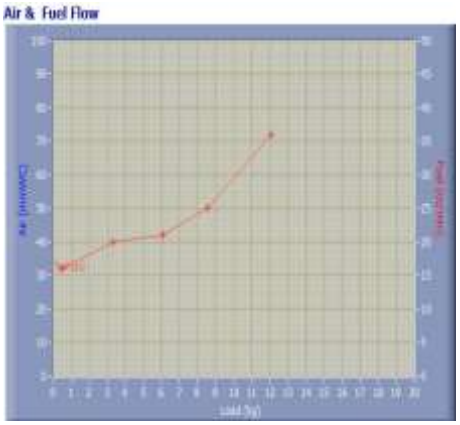

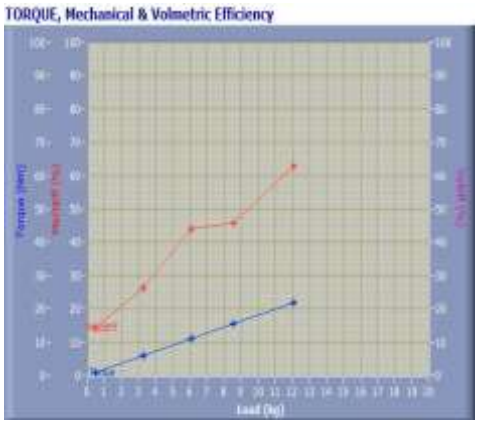

Indicated power (IP), brake power (BP) and friction power (FP).

Speed (rpm)	Load (kg)	IP (kW)	BP (kW)	FP (kW)
1261.00	0.46	0.77	0.11	0.66
1260.00	3.28	2.98	0.79	2.19
1261.00	6.08	3.31	1.46	1.85
1240.00	8.54	4.39	2.01	2.38
1175.00	12.06	4.29	2.69	1.59

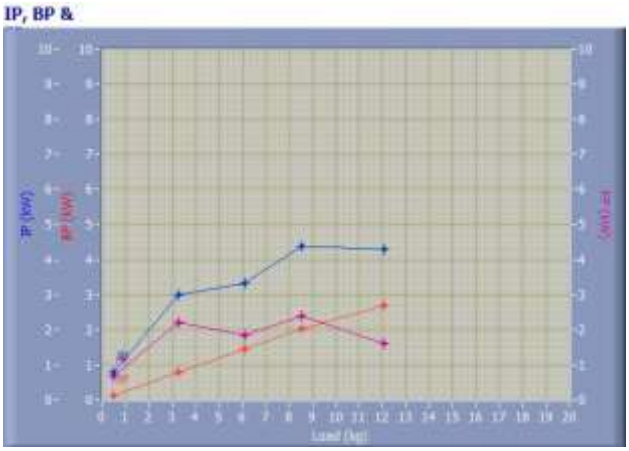

Observation Data

Speed (rpm)	Load (kg)	Comp Ratio	T1 (deg C)	T2 (deg C)	T3 (deg C)	T4 (deg C)	T5 (deg C)	T6 (deg C)
1261	0.46	100.00	22.44	26.39	22.43	24.48	313.79	258.68
1260	3.28	100.00	22.42	26.56	22.41	24.40	361.49	271.25
1261	6.08	100.00	22.39	26.88	22.39	24.69	429.35	312.31
1240	8.54	100.00	22.38	27.21	22.37	24.95	464.22	338.92
1175	12.06	100.00	22.35	27.78	22.35	25.20	476.96	352.02

Observation Data

Air (mmWC)	Fuel (cc/min)	WaterFlow Engine (lph)	WaterFlow Cal (lph)
266.78	16.00	250	150
266.80	20.00	250	150
266.77	21.00	250	150
266.80	25.00	250	150
266.80	36.00	250	150

Results Data

Torque (Nm)	BP (kW)	FP (kW)	IP (kW)	BMEP (bar)	IMEP (bar)	BTHE (%)	ITHE (%)	Mech Eff. (%)
0.84	0.11	0.66	0.77	0.16	1.11	1.19	8.30	14.29
5.95	0.79	2.19	2.98	1.13	4.29	6.76	25.63	26.38
11.03	1.46	1.85	3.31	2.10	4.76	11.94	27.13	44.02
15.50	2.01	2.38	4.39	2.94	6.42	13.86	30.22	45.85
21.89	2.69	1.59	4.29	4.16	6.62	12.88	20.50	62.84

Results Data

Air Flow (kg/h)	Fuel Flow (kg/h)	SFC (kg/kWh)	Vol Eff. (%)	A/F Ratio	HBP (%)	HJW (%)	HGas (%)	HRad (%)
53.19	0.80	7.22	181.08	66.76	1.19	12.36	50.89	35.56
53.19	1.00	1.27	181.23	53.41	6.76	10.35	47.66	35.23
53.19	1.05	0.72	181.08	50.86	11.94	10.71	54.65	22.70
53.19	1.25	0.62	184.16	42.73	13.86	9.68	50.07	26.39
53.19	1.79	0.67	194.34	29.67	12.88	7.55	36.14	43.43

OCB20

Indicated & Brake Thermal Efficiency and SFC & Fuel Consumption

Speed (rpm)	Load (kg)	IThEff (%)	BThEff (%)	SFC (kg/kWh)	Fuel (kg/h)
1249.00	0.37	13.93	0.79	1.10	0.95
1246.00	3.21	20.03	5.69	0.15	1.15
1241.00	6.21	21.70	12.08	0.08	1.25
1221.00	9.14	25.11	13.21	0.05	1.20
1134.00	12.20	16.57	10.28	0.08	2.19

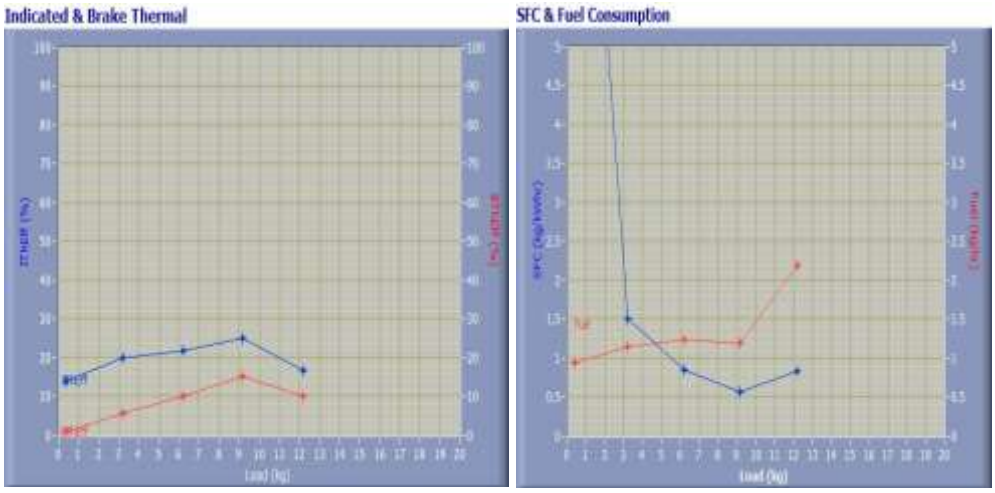

Air & Fuel Flow and Torque, Mechanical & Volumetric Efficiency

Speed (rpm)	Load (Kg)	Air (mmWC)	Fuel (cc/min)	Torque (Nm)	Mech Eff. (%)	Vol Eff. (%)
1249.00	0.37	266.81	19.00	0.66	5.64	182.83
1246.00	3.21	266.81	23.00	5.83	28.40	183.27
1241.00	6.21	266.81	25.00	11.26	46.45	184.01
1221.00	9.14	266.78	24.00	16.59	60.58	187.02
1134.00	12.20	266.78	44.00	22.13	62.05	201.36

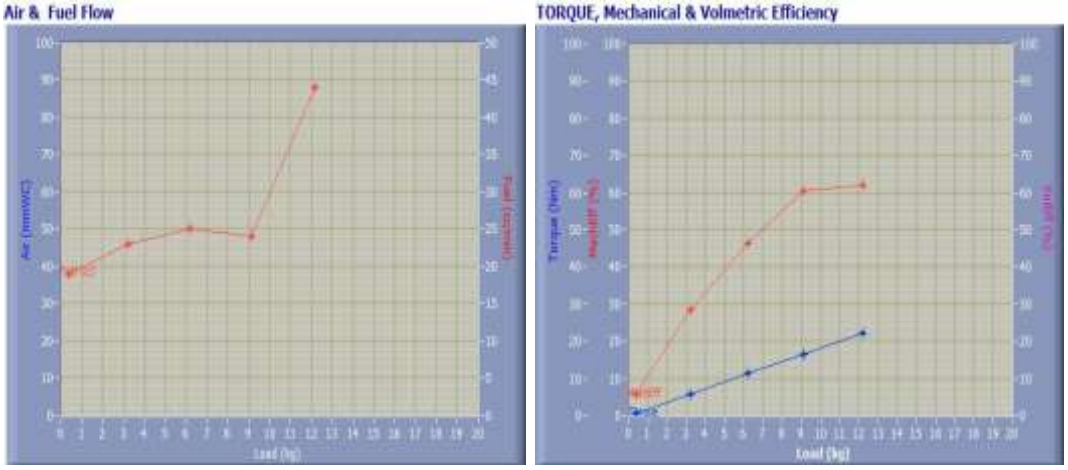

Indicated power (IP), brake power (BP) and friction power (FP).

Speed (rpm)	Load (kg)	IP (kW)	BP (kW)	FP (kW)
1249.00	0.37	1.54	0.09	1.45
1246.00	3.21	2.68	0.76	1.92
1241.00	6.21	3.15	1.46	1.69
1221.00	9.14	3.50	2.12	1.38
1134.00	12.20	4.24	2.63	1.61

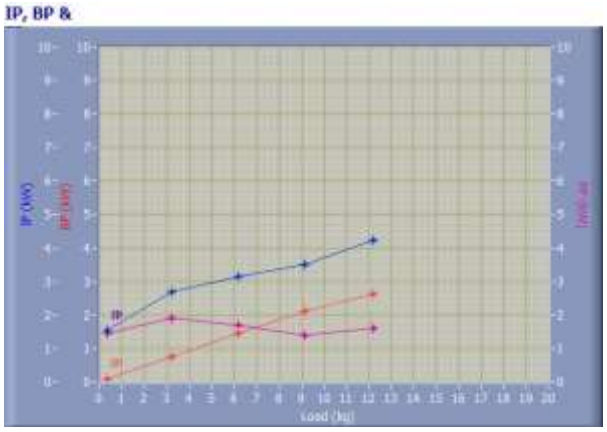

Observation Data

Speed (rpm)	Load (kg)	Comp Ratio	T1 (deg C)	T2 (deg C)	T3 (deg C)	T4 (deg C)	T5 (deg C)	T6 (deg C)
1249	0.37	100.00	23.82	111.30	23.86	24.60	316.64	249.96
1246	3.21	100.00	23.84	111.30	23.86	24.72	346.08	265.55
1241	6.21	100.00	23.85	111.30	23.89	24.87	393.91	304.29
1221	9.14	100.00	23.87	111.30	23.89	24.96	409.66	314.59
1134	12.20	100.00	23.87	111.30	23.90	25.09	447.26	332.92

Observation Data

Air (mmWC)	Fuel (cc/min)	Water Flow Engine (lph)	Water Flow Cal (lph)
266.81	19.00	0	0
266.81	23.00	0	0
266.81	25.00	250	150
266.78	24.00	250	150
266.78	44.00	250	150

Results Data

Torque (Nm)	BP (kW)	FP (kW)	IP (kW)	BMEP (bar)	IMEP (bar)	BTHE (%)	ITHE (%)	Mech Eff. (%)
0.66	0.09	1.45	1.54	0.13	2.23	0.79	13.93	5.64
5.83	0.76	1.92	2.68	1.11	3.90	5.69	20.03	28.40
11.26	1.46	1.69	3.15	2.14	4.61	10.08	21.70	46.45
16.59	2.12	1.38	3.50	3.15	5.20	15.21	25.11	60.58
22.13	2.63	1.61	4.24	4.20	6.78	10.28	16.57	62.05

OCB20-GNP50

Indicated & Brake Thermal Efficiency and SFC & Fuel Consumption

Speed (rpm)	Load (kg)	IThEff (%)	BThEff (%)	SFC (kg/kWh)	Fuel (kg/h)
1335.00	0.30	-60.81	1.02	0.84	0.65
1264.00	3.32	7.80	6.87	0.18	1.00
1260.00	6.20	26.39	11.61	0.07	1.10
1234.00	9.04	27.98	13.51	0.06	1.34

1167.00	11.82	20.47	11.87	0.07	1.89

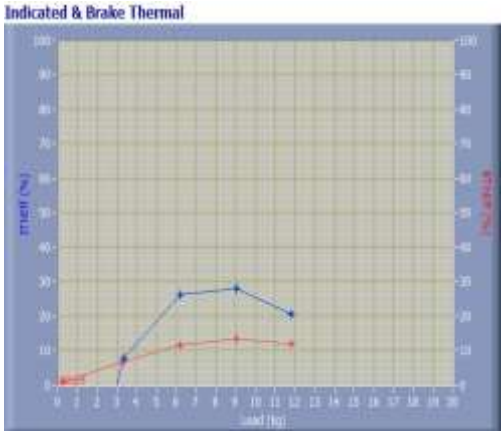

Air & Fuel Flow and Torque, Mechanical & Volumetric Efficiency

Speed (rpm)	Load (kg)	Air (mmWC)	Fuel (cc/min)	Torque (Nm)	Mech Eff. (%)	Vol Eff. (%)
1335.00	0.30	266.81	13.00	0.55	0.00	171.06
1264.00	3.32	266.79	20.00	6.03	88.09	180.66
1260.00	6.20	266.79	22.00	11.25	44.00	181.23
1234.00	9.04	266.81	27.00	16.40	48.30	185.06
1167.00	11.82	266.79	38.00	21.45	58.00	195.67

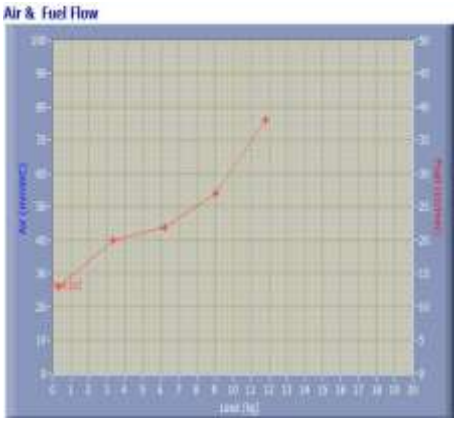

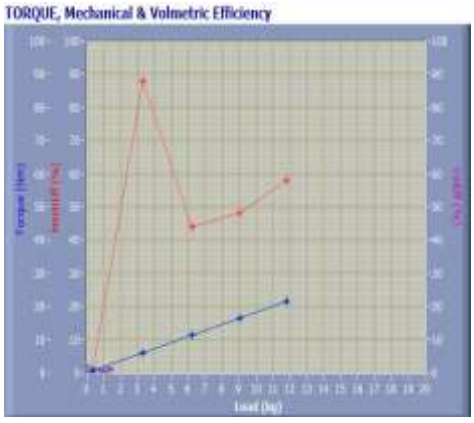

Indicated power (IP), brake power (BP) and friction power (FP)

Speed (rpm)	Load (kg)	IP (kW)	BP (kW)	FP (kW)
1335.00	0.30	-4.59	0.08	0.00
1264.00	3.32	0.91	0.80	0.11
1260.00	6.20	3.37	1.48	1.89
1234.00	9.04	4.39	2.12	2.27
1167.00	11.82	4.52	2.62	1.90

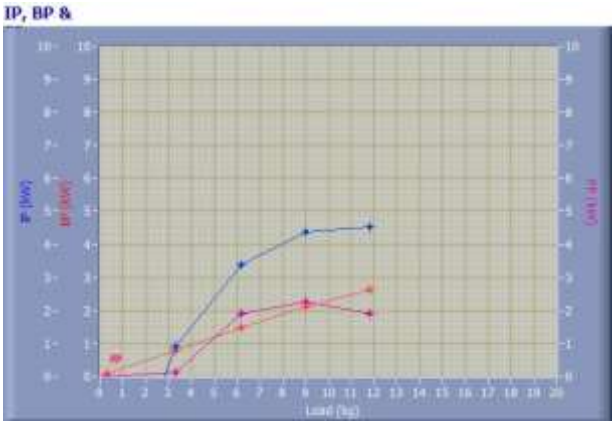

Observation Data

Speed (rpm)	Load (kg)	Comp Ratio	T1 (deg C)	T2 (deg C)	T3 (deg C)	T4 (deg C)	T5 (deg C)	T6 (deg C)
1335	0.30	100.00	22.72	24.37	22.70	23.41	212.75	147.15
1264	3.32	100.00	22.74	25.46	22.74	24.01	325.91	216.26
1260	6.20	100.00	22.75	26.32	22.76	24.58	395.95	275.48
1234	9.04	100.00	22.77	27.04	22.78	25.00	441.18	315.14
1167	11.82	100.00	22.79	27.78	22.78	25.38	464.45	336.86

Observation Data

Air (mmWC)	Fuel (cc/min)	Water Flow Engine (lph)	Water Flow Cal (lph)
266.81	13.00	250	150
266.79	20.00	250	150
266.79	22.00	250	150
266.81	27.00	250	150
266.79	38.00	250	150

Results Data

Torque (Nm)	BP (kW)	FP (kW)	IP (kW)	BMEP (bar)	IMEP (bar)	BTHE (%)	ITHE (%)	Mech Eff. (%)
0.55	0.08	0.00	-4.59	0.10	-6.24	1.02	-60.81	0.00
6.03	0.80	0.11	0.91	1.15	1.30	6.87	7.80	88.09
11.25	1.48	1.89	3.37	2.14	4.86	11.61	26.39	44.00
16.40	2.12	2.27	4.39	3.12	6.45	13.51	27.98	48.30
21.45	2.62	1.90	4.52	4.07	7.03	11.87	20.47	58.00

Results Data

Air Flow (kg/h)	Fuel Flow (kg/h)	SFC (kg/kWh)	Vol Eff. (%)	A/F Ratio	HBP (%)	HJW (%)	HGas (%)	HRad (%)
53.20	0.65	8.41	171.06	82.17	1.02	6.37	40.46	52.15
53.19	1.00	1.25	180.66	53.41	6.87	6.81	42.59	43.72
53.19	1.10	0.74	181.23	48.55	11.61	8.10	47.88	32.40

53.19	1.34	0.63	185.06	39.56	13.51	7.91	44.00	34.58
53.19	1.89	0.72	195.67	28.11	11.87	6.58	33.35	48.20

OCB20-GNP75

Speed (rpm)	Load (kg)	IThEff (%)	BThEff (%)	SFC (kg/kWh)	Fuel (kg/h)
1271.00	0.27	7.95	0.70	1.23	0.80
1266.00	3.28	18.36	6.79	0.13	1.00
1261.00	6.40	27.06	13.21	0.07	1.00
1250.00	8.80	29.99	13.84	0.06	1.29
1178.00	11.68	19.04	12.85	0.07	1.74

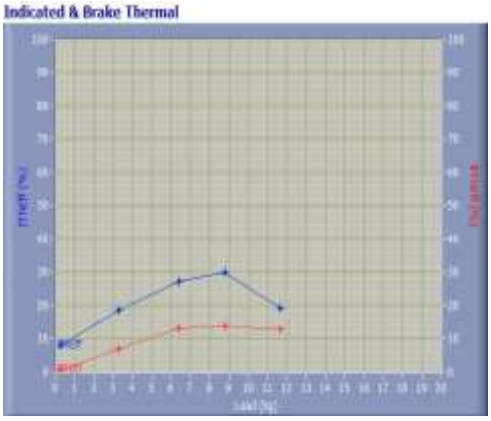

Air & Fuel Flow and Torque, Mechanical & Volumetric Efficiency

Speed (rpm)	Load (Kg)	Air (mmWC)	Fuel (cc/min)	Torque (Nm)	Mech Eff. (%)	Vol Eff. (%)
1271.00	0.27	266.82	16.00	0.49	8.77	179.67
1266.00	3.28	266.80	20.00	5.95	36.96	180.38
1261.00	6.40	266.82	20.00	11.62	48.80	181.10
1250.00	8.80	266.80	26.00	15.98	46.17	182.68
1178.00	11.68	266.79	35.00	21.19	67.53	193.85

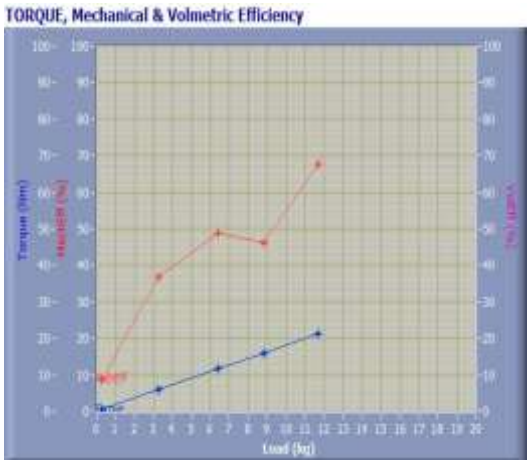

Indicated power (IP), brake power (BP) and friction power (FP).

Speed (rpm)	Load (kg)	IP (kW)	BP (kW)	FP (kW)
1271.00	0.27	0.74	0.06	0.67
1266.00	3.28	2.13	0.79	1.35
1261.00	6.40	3.14	1.53	1.61
1250.00	8.80	4.53	2.09	2.44
1178.00	11.68	3.87	2.61	1.26

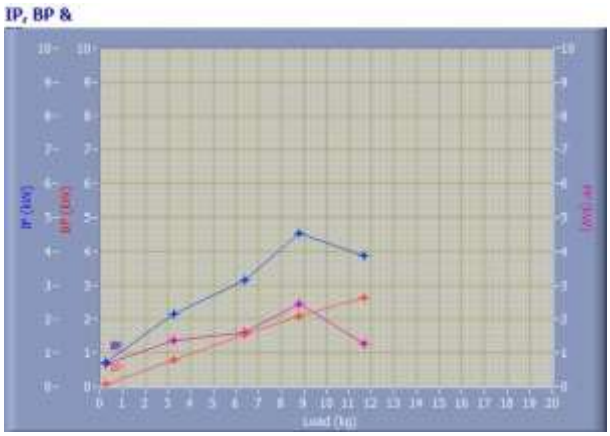

Observation Data

Speed (rpm)	Load (kg)	Comp Ratio	T1 (deg C)	T2 (deg C)	T3 (deg C)	T4 (deg C)	T5 (deg C)	T6 (deg C)
1271	0.27	100.00	22.74	25.62	22.73	24.00	263.72	194.14
1266	3.28	100.00	22.74	25.99	22.73	24.29	334.16	237.38
1261	6.40	100.00	22.73	26.40	22.74	24.59	377.31	272.61
1250	8.80	100.00	22.73	27.07	22.73	24.93	436.83	309.34
1178	11.68	100.00	22.73	27.86	22.72	25.30	466.71	333.69

Observation Data

Air (mmWC)	Fuel (cc/min)	WaterFlow Engine (lph)	WaterFlow Cal (lph)
266.82	16.00	250	150
266.80	20.00	250	150
266.82	20.00	250	150
266.80	26.00	250	150
266.79	35.00	250	150

Results Data

Torque (Nm)	BP (kW)	FP (kW)	IP (kW)	BMEP (bar)	IMEP (bar)	BTHE (%)	ITHE (%)	Mech Eff. (%)
0.49	0.06	0.67	0.74	0.09	1.06	0.70	7.95	8.77
5.95	0.79	1.35	2.13	1.13	3.06	6.79	18.36	36.96
11.62	1.53	1.61	3.14	2.21	4.52	13.21	27.06	48.80
15.98	2.09	2.44	4.53	3.04	6.57	13.84	29.99	46.17
21.19	2.61	1.26	3.87	4.03	5.96	12.85	19.04	67.53

Results Data

Air Flow (kg/h)	Fuel Flow (kg/h)	SFC (kg/kWh)	Vol Eff. (%)	A/F Ratio	HBP (%)	HJW (%)	HGas (%)	HRad (%)
53.20	0.80	12.29	179.67	66.76	0.70	9.03	42.01	48.26
53.19	1.00	1.26	180.38	53.41	6.79	8.13	43.77	41.32
53.20	1.00	0.65	181.10	53.41	13.21	9.16	49.92	27.71
53.19	1.29	0.62	182.68	41.08	13.84	8.35	45.17	32.64
53.19	1.74	0.67	193.85	30.52	12.85	7.33	36.30	43.52

OCB20-GNP100

Indicated & Brake Thermal Efficiency and SFC & Fuel Consumption

Speed (rpm)	Load (kg)	IThEff (%)	BThEff (%)	SFC (kg/kWh)	Fuel (kg/h)
1276.00	0.24	6.52	0.66	1.29	0.75
1266.00	3.28	24.24	6.79	0.13	1.00
1259.00	6.48	29.70	12.14	0.07	1.10
1234.00	8.92	21.92	13.34	0.06	1.34
1178.00	11.74	20.97	12.22	0.07	1.84

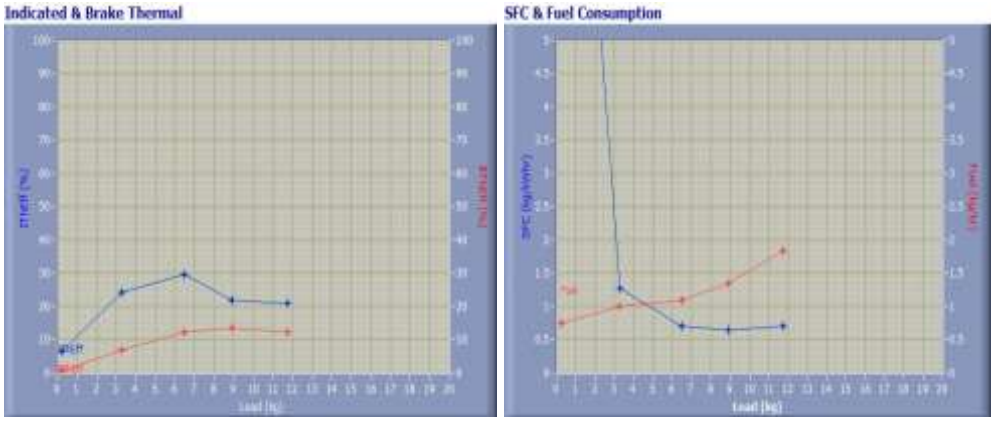

Air & Fuel Flow and Torque, Mechanical & Volumetric Efficiency

Speed (rpm)	Load (kg)	Air (mmWC)	Fuel (cc/min)	Torque (Nm)	Mech Eff. (%)	Vol Eff. (%)
1276.00	0.24	266.75	15.00	0.43	10.20	178.95
1266.00	3.28	266.77	20.00	5.95	28.03	180.36
1259.00	6.48	266.78	22.00	11.77	40.88	181.37
1234.00	8.92	266.78	27.00	16.19	60.84	185.04
1178.00	11.74	266.76	37.00	21.30	58.30	193.83

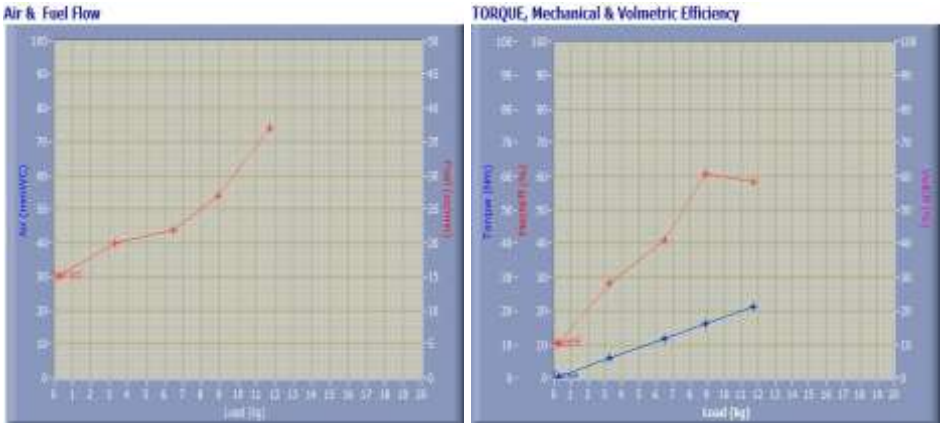

Indicated power (IP), brake power (BP) and friction power (FP).

Speed (rpm)	Load (kg)	IP (kW)	BP (kW)	FP (kW)
1276.00	0.24	0.57	0.06	0.51
1266.00	3.28	2.82	0.79	2.03
1259.00	6.48	3.80	1.55	2.24
1234.00	8.92	3.44	2.09	1.35
1178.00	11.74	4.51	2.63	1.88

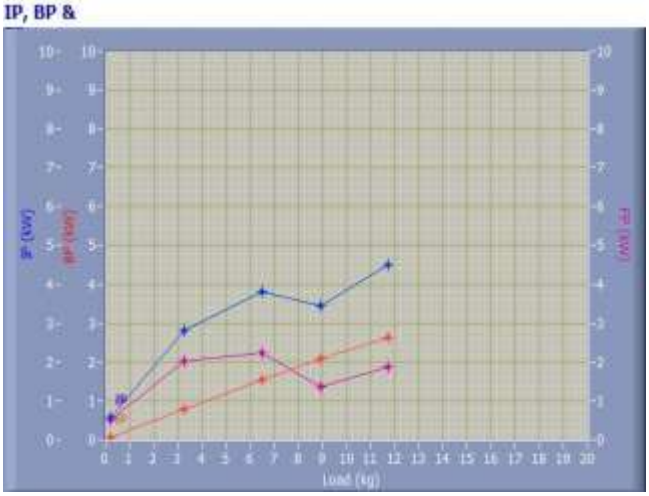

Observation Data

Speed (rpm)	Load (kg)	Comp Ratio	T1 (deg C)	T2 (deg C)	T3 (deg C)	T4 (deg C)	T5 (deg C)	T6 (deg C)
1276	0.24	100.00	22.87	25.80	22.87	24.08	241.00	185.98
1266	3.28	100.00	22.89	26.08	22.89	24.31	324.69	226.17
1259	6.48	100.00	22.89	26.78	22.90	24.78	396.13	275.58
1234	8.92	100.00	22.91	27.60	22.91	25.24	452.73	317.44
1178	11.74	100.00	22.92	44.12	22.92	25.52	470.85	336.13

Observation Data

Air (mmWC)	Fuel (cc/min)	WaterFlow Engine (lph)	WaterFlow Cal (lph)
266.75	15.00	2500	150
266.77	20.00	2500	150
266.78	22.00	2500	150
266.78	27.00	2500	150
266.76	37.00	2500	150

Results Data

Torque (Nm)	BP (kW)	FP (kW)	IP (kW)	BMEP (bar)	IMEP (bar)	BTHE (%)	ITHE (%)	Mech Eff. (%)
0.43	0.06	0.51	0.57	0.08	0.81	0.66	6.52	10.20
5.95	0.79	2.03	2.82	1.13	4.04	6.79	24.24	28.03
11.77	1.55	2.24	3.80	2.24	5.47	12.14	29.70	40.88
16.19	2.09	1.35	3.44	3.08	5.06	13.34	21.92	60.84
21.30	2.63	1.88	4.51	4.05	6.94	12.22	20.97	58.30

Results Data

Air Flow (kg/h)	Fuel Flow (kg/h)	SFC (kg/kWh)	Vol Eff. (%)	A/F Ratio	HBP (%)	HJW (%)	HGas (%)	HRad (%)
53.19	0.75	12.90	178.95	71.20	0.66	97.96	40.47	0.00
53.19	1.00	1.26	180.36	53.40	6.79	79.89	42.42	0.00
53.19	1.10	0.71	181.37	48.55	12.14	88.39	47.90	0.00
53.19	1.34	0.64	185.04	39.56	13.34	86.92	45.22	0.00
53.19	1.84	0.70	193.83	28.87	12.22	286.80	34.72	0.00